NON-SINUSOIDAL CURRENT-PHASE RELATIONS IN SUPERCONDUCTOR-FERROMAGNET-SUPERCONDUCTOR JOSEPHSON JUNCTIONS

BY

MICAH JOHN ATMAN STOUTIMORE

B.S., University of Florida, 2001
M.S., University of Illinois at Urbana-Champaign, 2004

DISSERTATION

Submitted in partial fulfillment of the requirements
for the degree of Doctor of Philosophy in Physics
in the Graduate College of the
University of Illinois at Urbana-Champaign, 2009

Urbana, Illinois

Doctoral Committee:

Associate Professor Alexey Bezryadin, Chair
Professor Dale J. Van Harlingen, Director of Research
Professor Michael Stone
Professor Steven M. Errede

Acknowledgments

I would like to thank my advisor, Dale Van Harlingen, without whom this thesis surely would never have been completed. Under Dale's leadership, I learned nearly everything I know about experimental physics. I learned the value of difficult projects, as well as the importance of knowing when to say "no." Sergey Frolov also directly contributed to this thesis by introducing me and Dale to Valery Ryazanov and the wonderful physics of superconductor-ferromagnet-superconductor junctions. Both Sergey and Valery have played an integral role in the work I present here.

In the winter of 2007, Alexander "Sasha" Rusanov came to the University of Illinois with two samples and an immeasurable amount of energy. Together we performed much of the direct current-phase measurement that is presented in chapter six. I thank him for his enthusiasm and friendship.

Other members of the DVH research group have contributed to my education in countless ways. Trevis Crane introduced me to the group and to microfabrication. Joel Strand has not only discussed my own work with me, but has also allowed me to express my thoughts about his own research whenever I needed to think about something different. Dan Bahr is always available to lend a hand for anything. Francoise Kidwingira and Madalina Colci both began their journeys through graduate school and the DVH group with me, and it has been a pleasure to be in their company for all these years. William (Bill) Neils, David Caplan and Martin Stehno all have made this experience better. Though our time only overlapped marginally, I would like to wish good luck to the newest members of the group – Juan Atkinson, Chris Nugroho and Adam Weis.

There are many other people who have crossed paths with me at the University

of Illinois. In particular, I would like to thank Joe Altepeter, Evan Graves and Evan Jeffrey who taught me many things about science and about life. In particular, they taught me to appreciate and desire creativity and drive, duty, and staggering intelligence. Josh Rubin shared this experience with me starting from our first office and ending with our overlapping thesis depositions. He and I have discussed everything up to and including the nature of existence. His artistic aesthetic and intuition have served him amazingly well these past years and I only hope that some of it stays with me as I go forward.

My mother, Jolenea Ferro, father, Mike Stoutimore and stepmother, Terri Rodgers, have all encouraged and helped me. Rather than attempting to enumerate their contributions, I will simply say that I am certain that it was their guidance that led me to seek out what Truth I could find in the world of physics. My brother, Zack, has reminded me that there are other ways to seek truth. I know of no one else with his dedication to being good and doing right.

My wife, Amy, has shown me in the last several months that she has more patience than I have ever given her credit for. I can't imagine what this experience would have been like without her encouragement and her calming presence. She truly is my heart.

This work was supported by the National Science Foundation grant DMR-07-05214 and by the U.S. Civilian Research and Development Foundation grant RP1-2413-CG-02.

Contents

Chapter 1

Motivations

1.1 Formulation of the question

In Josephson junctions, the physical explanation of the supercurrent $j_s = j_c sin\phi$ is the local, coherent transport of a pair of electrons. Processes consisting of the coherent transport of 4 (or 6, or 8, etc.) electrons could also occur. In that case, the local pairing wavefunction would result in a current-phase relation of the form:

$$j_s(\phi) = \sum_{n=1}^{\infty} j_{cn} sin(n\phi). \tag{1.1}$$

where n represents the number of pairs involved in the tunneling process and the magnitude of j_{cn} is associated with the relative likelihood of that process.

The reality has been that most experiments related to the phase dynamics are explained by the $sin\phi$ term alone.

The question that motivates the experiments in this thesis is: "Can diffusive superconductor-ferromagnet-superconductor (SFS) junctions be used to definitively identify the coherent transport of multiple Cooper pairs, leading to a local current-phase relation proportional to $sin(2\phi)$"?

Learning the answer gives insight into the physical picture of the Josephson effect and, consequently, superconductivity. If there is a fundamental physical reason that those terms cannot appear in real systems, then there may be a

mechanism that suppresses them which we do not understand.

The small probabilities associated with second- and higher-order terms relative to the first-order term is sufficient in most Josephson junctions to prevent us from measuring it. In SFS junctions the first-order term can vanish due to interaction with the superconducting state with the ferromagnetism, and it has been suggested that the second-harmonic term could become dominant.

1.2 Explanation of the contradictions

Published experiments have claimed to show this effect, both in superconductor–normal-metal–superconductor (SNS) and SFS junctions, and results from the Van Harlingen group suggest that the technique used to identify the higher harmonics could also lead to results due to spatial variations in the barrier thickness.

The model proposed by Sergey Frolov and Dale Van Harlingen was based on an analogy with a conventional dc-SQUID is a half-flux quantum magnetic field. An extension of the model to a more rapidly varying phase difference across the width of the barrier was proposed by Mints and has been extensively reviewed by both Mints and Buzdin. Their model predicts that the term proportional to $sin(2\phi)$ will be negative and much larger than the local second-harmonic term.

1.3 Formulation of the solution

We believe that to make significant statements about the source of second harmonics, it is necessary to directly measure the current phase relations, which is capable of resolving the sign of that term. Also, it's necessary to perform the usual transport measurements, to look for the temperature dependence of second harmonics and to rule out non-uniformities of the scale that we measured in previous junctions. With that in mind, we fabricated a sample in a superconducting loop for direct current-phase measurement.

Chapter 2

Superconductivity

Here we will introduce the basic concepts of superconductivity and develop the formalism needed to understand the significance of the work presented in the later chapters.

2.1 Basic concepts

In 1911, shortly after developing a technique for condensing helium into its liquid state, Kamerlingh Onnes [1] measured the resistivity of the element mercury and discovered that it abruptly fell to zero at a critical temperature, T_c. The mercury had undergone a phase transition into the newly realized superconducting state. Current flow without resistance is referred to as the supercurrent throughout.

In addition to exhibiting zero electrical resistance, superconducting materials expel magnetic fields from the bulk for small enough values of field, called the Meissner effect [2]. The fields penetrate into bulk superconductors up to a characteristic length, λ, known as the penetration depth.

Normally, the ground state of a non-interacting gas of electrons (a simple model for electronic states in metals) is made up of electrons filling discrete momentum states, p, with energy $E_p = p^2/2m$ up to the Fermi energy, $E_F = p_F^2/2m$. An excited state is constructed by removing an electron from its momentum state and placing it into a higher energy momentum state, $p' > p_F$. The

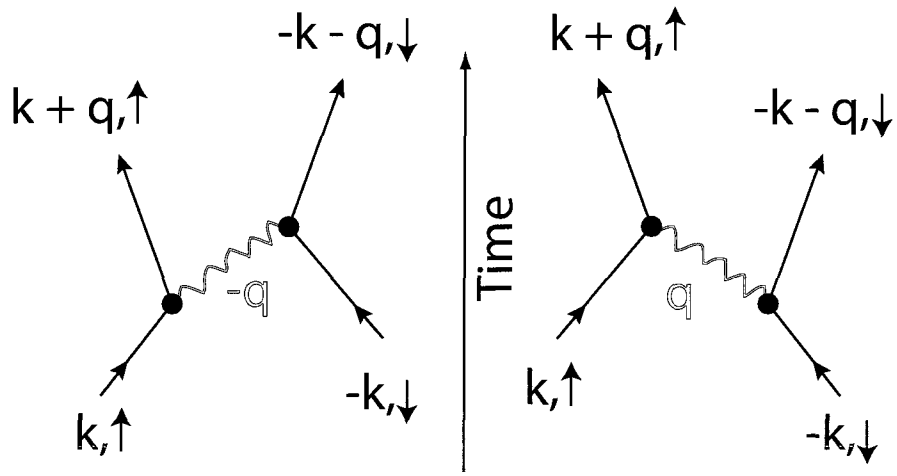

Figure 2.1: Diagram showing the possible electron-electron interaction modes mediated by the exchange of a phonon (in red) for Cooper pairs.

energy difference between this excited state and the ground state from which it was constructed can be very small if p and p' are both near the Fermi momentum.

In normal metals, these low-energy excitations of electron-hole pairs occur frequently. Once a material enters the superconducting state, however, these low-energy excited states cease to exist. In that case, the lowest energy excitations occur at a characteristic energy of 2Δ for an electron-hole pair, Δ per excitation. This effect is shown in several experiments, including the exponential nature of specific heat ($exp(-\Delta/k_BT)$), the minimum energy for photon absorbtion ($\hbar\omega \geq 2\Delta$) and in tunneling experiments between a superconductor and normal metal separated by a thin insulating barrier where the minimum voltage required for electron transport is such that the electron energy gains $eV \geq \Delta$.

2.1.1 Cooper pairs

The non-interacting free electron gas model of the normal state becomes unstable if an attractive interaction is allowed [3]. Instead, electrons combine to form a bound state that behaves as a boson. The instability in the normal state persists even for very small interaction potentials as long as it remains attractive.

The Bardeen/Cooper/Schrieffer (BCS) [4] theory of superconductivity helped

to elucidate the origin of the attractive potential. In the simple picture of a free electron gas, the only interaction present is Coulomb repulsion among the like-charged electrons. In order to identify the source of the attractive potential, we must introduce interaction with a system other than the electron gas. For the case of low critical temperature superconductors, electron-phonon interactions provide the neccessary attractive potential.

Figure 2.1 shows the processes of electron-electron coupling via a phonon. In both cases, the electrons start in an inital state $\mathbf{k}$, -$\mathbf{k}$ and end in a final state $\mathbf{k'}$, -$\mathbf{k'}$ where $k' = k + q$.

A qualitative picture of the phonon-mediated electron-electron interaction is based on the jellium model of a metal that was applied to superconductivity first by Pines [5]. In this model, the metal is made up of a uniform density of electrons and heavier ions. The neccessary attractive potential between electrons 1 and 2 occurs due to screening of the Coulomb repulsion by the positive ions in the lattice. Electron 1 attracts a cloud of surrounding positive ions. If the attraction occurs near the resonance frequency of the lattice motion, then the ions can effectively over-screen, creating an effective positive charge to which electron 2 is attracted.

Because the Cooper pair model depends on interactions with the lattice, different isotopes of the same material should show slightly different superconducting transition temperatures. Known as the isotope effect, this was first observed by [6, 7], proving that lattice interaction does play a strong role in Cooper pairing.

2.1.2 Phase coherence

Prior to the BCS theory, Ginzburg and Landau published a phenomenological model for superconductivity [8] based on previous work by Landau on general phase transition phenomenology. The theory relies on identifying an ordering process associated with the phase transition. In the case of superconductivity, the ordering is the condensing of electron states into Cooper pairs as described in the previous section. Therefore, the order parameter characterizing superconductivity is defined

as the number of pairs, n_p.

With this order parameter, they set out to find the appropriate free energy as a function of the parameter, $F(n_p, T)$. By assuming that the free energy can be expanded near the transition temperature, T_c, in powers of n_p, they were able to solve for the free energy and thereby make predictions for the behavior of the free energy density, heat capacity and critical field.

This mean field theory is only valid if there are small fluctuations – not a safe assumption for higher-order transitions. Fortunately, due to the large size of the Cooper pairs much of the fluctuations can be averaged out.

Based on the success of the London model [9] which assumed that superconductivity could be explained using a wavefunction description, Ginzburg and Landau went further and introduced a complex order parameter, ψ, such that $\psi^*\psi = n_p$. While this complex parameter cannot be strictly interpreted as a wavefunction, its phase evolves in the same way as the phase of a wavefunction for a charged particle. Throughout this thesis, references to the superconducting wavefunction are equivalent to this complex order parameter and have the form:

$$\psi(r) = \sqrt{n_p} e^{i\theta(r)} = \psi_0 e^{i\theta(r)}. \tag{2.1}$$

The phase, ϕ, is a gauge covariant quantity, meaning it can have an arbitrary offset at any point in the superconductor.

2.1.3 Fluxoid quantization

The Ginzburg-Landau theory for zero resistance supercurrents is defined in terms of the superconducting order parameter and vector potential by the following equation:

$$\begin{aligned} J_s &= \frac{ie\hbar}{m}(\psi^*\nabla\psi - \psi\nabla\psi^*) - \frac{4e^2}{m}A\psi^*\psi \\ &= -\frac{4e^2 n_p}{m}(\frac{\hbar}{2e}\nabla\theta + A), \end{aligned} \tag{2.2}$$

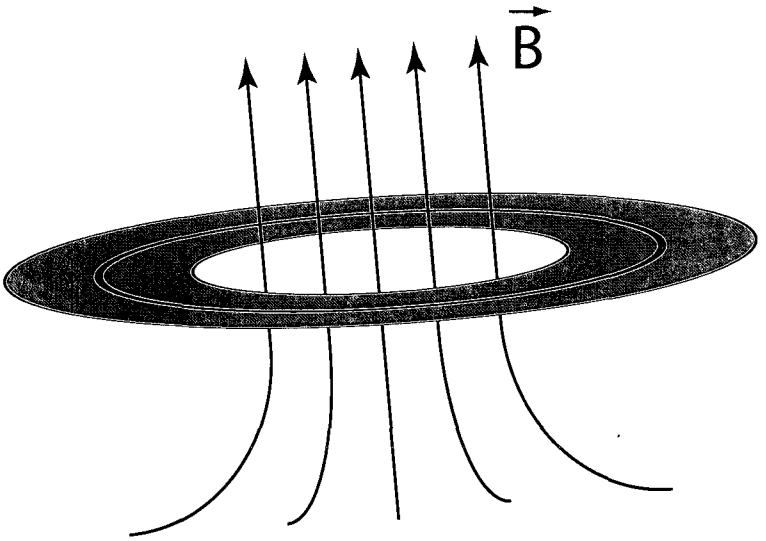

Figure 2.2: When considering the phase change around a superconducting loop (blue) with enclosed field, we derive the condition of fluxoid quantization. If the integration path (black) is sufficiently far from the edges of the superconducting ring, then the equation simplifies to give flux quantization in integral multiples of $\Phi_0 = 20.7\text{Gauss}\cdot\mu\text{m}^2$.

where the second line follows from substituting equation 2.1 for ψ in the first line [10].

For a superconducting ring as in figure 2.2, if we wish to know the change in phase around the loop, we take a line integral of equation 2.2. For a well-defined phase, the integral of $\nabla\theta = 2\pi n$, where n is an integer. If the path of integration is more than a penetration depth away from the edges of the superconducting ring, then the current density equals zero and the the line integral reduces to

$$\frac{\hbar}{2e}2\pi n = \oint A \cdot dl = \Phi. \tag{2.3}$$

If we define $\Phi_0 = (h/2e)$, then we see from equation 2.3 that the flux, Φ, enclosed by the superconducting loop is an integer multiple of Φ_0, the magnetic flux quantum: $\Phi = n\Phi_0$.

The general case in which we do not neglect the supercurrent component, J_s, requires that the fluxoid, given by $\oint[A + (m/2n_p e^2)J_s] \cdot dl$, is quantized. Another important situation for this thesis will be the case of a superconducting ring

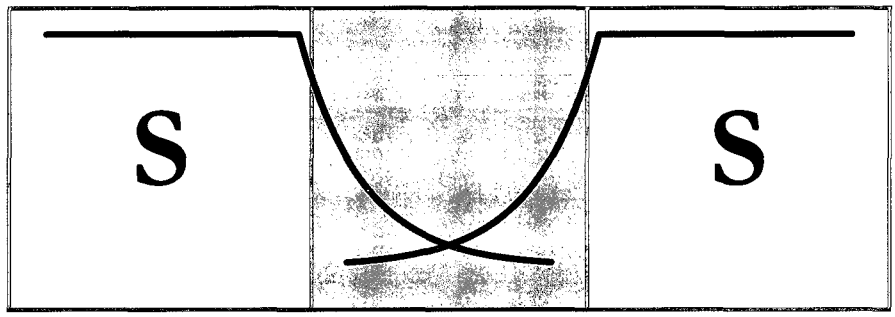

Figure 2.3: A schematic showing superconducting correlations from two superconducting electrodes extending into an adjacent material. If the wavefunction from the right, ψ_R, overlaps sufficiently with the wavefunction from the left, ψ_L, then supercurrent transfer occurs. This type of superconducting circuit is a Josephson junction.

interrupted by a Josephson junction, which we will show in detail in chapter 6.

2.2 Superconducting weak links

B.D. Josephson [11] predicted the phase-coherent tunneling of the superconducting state through an insulating link. The theory he derived has been extended to include other weak links such as superconducting constrictions and metals. Studying Josephson junctions has provided a way to understand the physics of the superconducting state as well as the interaction of superconductivity with other states of materials [12, 13].

2.2.1 Proximity effect

When a superconductor – like any highly order material – comes into contact with another material, the ordering should extend some distance into the new material. This means that Cooper pair correlations are induced in the adjacent media over a characteristic length scale dependent on the details of the material, as shown in figure 2.3.

As an example, for a superconductor–normal-metal (SN) interface, the superconducting wavefunction penetrates on the length scale defined by the inelastic

scattering length:

$$\xi_N^{clean} = \frac{\hbar v_F}{2\pi k_B T} \quad \text{clean limit} \tag{2.4}$$

$$\xi_N^{dirty} = \sqrt{\frac{\hbar D}{2\pi k_B T}} \quad \text{dirty limit} \tag{2.5}$$

where ξ_N is defined as the normal metal coherence length. In these equations, v_F is the Fermi velocity, k_B is the Boltzmann constant and D is the diffusion coefficient of the metal. In this context, the "clean" or ballistic limit is the case in which the electron mean free path, l, is greater than the thickness of the the normal metal, L. The "dirty" or diffusive limit occurs for $L > l$.

When another superconductor is brought in contact with the superconductor–barrier combination, then the phases of the left and right superconductors become coupled if the order parameters overlap.

2.2.2 Current-phase relation

When considering the supercurrent through a Josephson junction, we take it to be a function of the phase difference between the two superconducting electrodes, $\phi = \theta_L - \theta_R$. This current-phase relation (CPR), $I(\phi)$, must obey certain conditions.

First, the assumption of *weakly-coupled* superconductors means that the current is a periodic function of the phase difference. If the phase of one superconducting electrode is changed by an integer multiple of 2π, the current through the junction will return to the original state, $I(\phi) = I(\phi + 2\pi n)$. In contrast, the current in *strongly-coupled* superconductors is linearly related to changes is phase, so that any difference leads to a net current flow through the link, and it is not returned to the same state.

Secondly, the direction of current flow across the junction is related to the sign of the phase change, $I(-\phi) = -I(\phi)$. When combined with the first requirement, this leads to the result that the supercurrent must be zero for phase differences that

are integer multiples of π:

$$I(\pi) = I(\pi - 2\pi) = I(-\pi) = -I(\pi) \tag{2.6}$$

All of these lead to the result that zero current flow through the junction corresponds to zero phase change across the junction.

These conditions suggest a solution to the CPR of a junction proportional to $sin(\phi)$. Josephson calculated that the full form should be the simple sinusoidal function given by:

$$I_s(\phi) = I_c sin(\phi). \tag{2.7}$$

The coefficient, I_c, is the junction critical current – usually a positive function of temperature that corresponds to the maximum current that can pass through the junction before dissipative current sets in.

Ambegaokar and Baratoff [14] applied microscopic theory to the same type of superconductor–insulator–superconductor (SIS) tunnel junction geometry that Josephson had considered. They found the temperature dependence of I_c is given by $I_c(T) \propto \Delta(T) tanh(\Delta(T)/T)$, where $\Delta(T)$ is the temperature dependent energy gap in the single-electron density of states that is created as those electrons form Cooper pairs.

Figure 2.4 shows a qualitative graph of $I_c(T)$ that assumes the gap can be represented by the $T \rightarrow T_c$ approximation. In this limit, the slope of the $T \rightarrow 0$ part of the curve is not accurate, but the trend that the critical current increases monotonically as temperature decreases for a conventional Josephson junction is accurate. In chapter 3, we will show how an SFS junction can have a non-monotonic temperature dependence.

2.2.3 Energetics

To determine the energetics of the Josephson junction, we apply the usual time-dependent Schrodinger equation, $-i\hbar(\partial\psi/\partial t) = E\psi$. From the definition of the

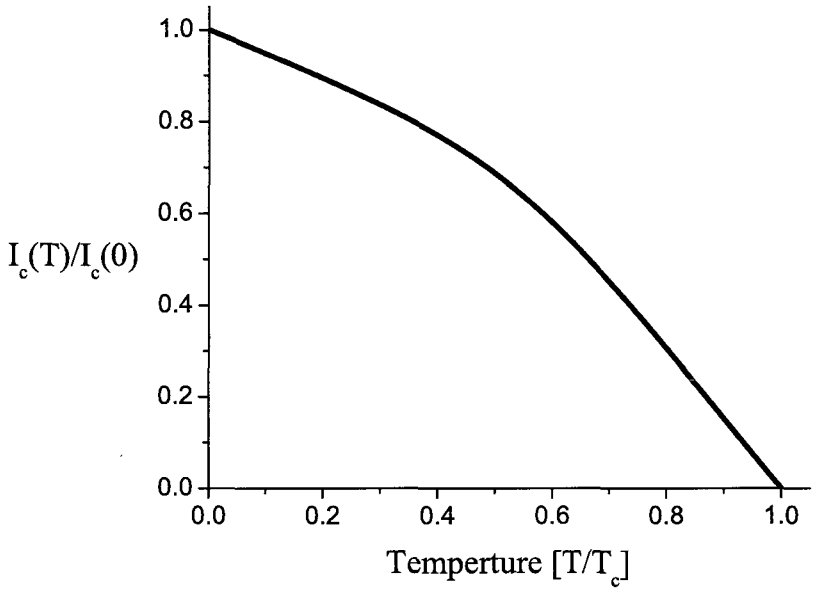

Figure 2.4: Temperature dependence of I_c based on the Ambegaokar-Baratoff microscopic theory giving $I_c(T) \propto \Delta(T)tanh(\Delta/2kT)$. The curve is only qualitative given that the gap value $\Delta(T)$ used to generate it is valid only near T_c.

Cooper pair wavefunction 2.1, the result is

$$\hbar\frac{\partial\phi}{\partial t} = -E = 2eV, \tag{2.8}$$

given that the energy imparted to a Cooper pair as it crosses a junction is the pair-charge multiplied by the voltage, V, maintained across the junction.

If we evolve the phase of the junction slowly and reversibly by applying a small voltage, then the free energy, F, is given by the time integral of the rate at which we are doing work:

$$\begin{aligned} F &= \int dt I_s V = \int d\phi I_c \frac{\hbar}{2e} sin\phi \\ &= \frac{\hbar I_c}{2e}(1 - cos\phi). \end{aligned} \tag{2.9}$$

The constant is chosen so that the energy is minimized for zero phase difference.

2.2.4 π-junctions

Josephson junctions that obey the CPR from equation 2.7 and whose energy is described accurately by equation 2.9 are what we will refer to as conventional or 0-junctions. Bulaevskii, Kuzii and Sobyanin [15] suggested the theoretical possibility of another type of Josephson junction, this one with a negative critical current. The negative sign of the critical current indicates that for small positive phase differences across the junction, the current flows opposite to the direction of the phase gradient. Such a junction has a CPR given by:

$$I_s(\phi) = -I_c sin\phi = I_c sin(\phi + \pi), \tag{2.10}$$

This junction is referred to as a Josephson π-junction because its CPR can be obtained by adding an intrinsic phase shift of π to the CPR of a conventional junction.

To derive this result, Bulaevskii *et al.* considered a tunnel junction containing magnetic impurities in the barrier. Spin-flip scattering of Cooper pair electrons has a negative contribution to the junction critical current because the amplitude of the order parameter must be inverted if the spin of one pair electron is flipped. In principle, if spin-flip tunneling could be made the dominant tunneling process, then the junction would become a π-junction. In practice, magnetic impurities tend to cause decoherence of Cooper pairs [16] and significantly depress the Josephson effect. As a result, a π-junction of this kind has never been measured experimentally.

Other systems that have been proposed as π-junctions include tunneling through a quantum dot [17, 18], through a normal-metal barrier with a non-equilibrium distribution of electrons in the barrier [19], through d-wave grain-boundary junctions [20, 21] and through a ferromagnetic barrier [22]. For each of these systems, a π-junction has been realized experimentally. The last of these four systems, the superconductor-ferromagnet-superconductor (SFS) junction, will be our focus.

The free energy of a junction with a CPR given by equation 2.10 has its energy

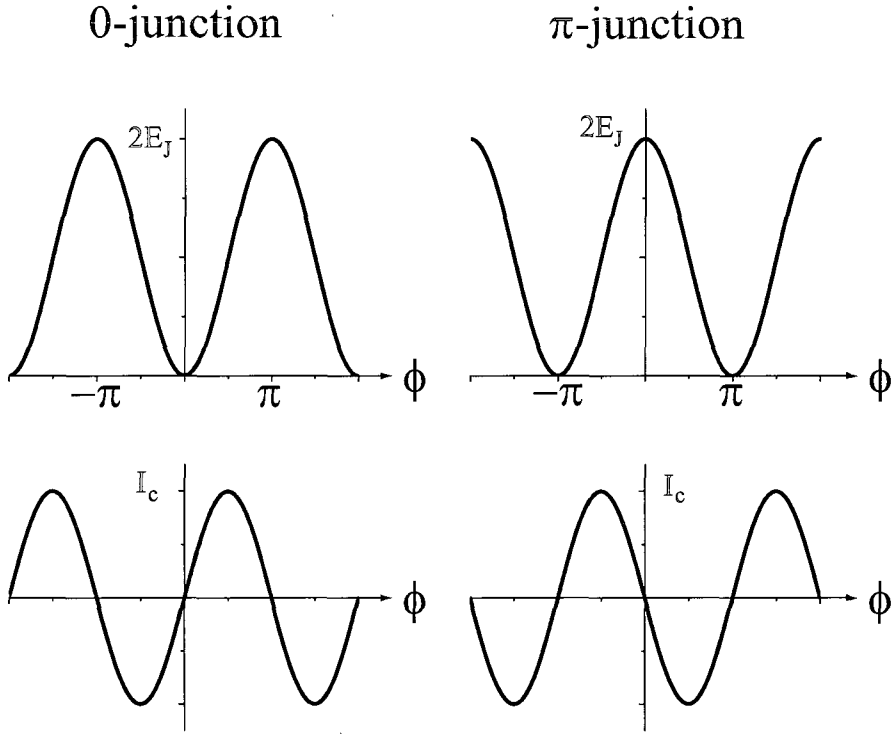

Figure 2.5: Plot of the energy, in the first row, and supercurrent, in the second row, as a function of the phase difference ϕ for a 0-junction and a π-junction.

minimum shifted as well:

$$F(\phi) = \frac{\hbar I_c}{2e}[1 - cos(\phi + \pi)] = \frac{\hbar I_c}{2e}[1 + cos(\phi)]. \tag{2.11}$$

Figure 2.5 shows graphically the energy and CPR of both a conventional 0-junction and a π-junction.

2.2.5 Higher-order harmonics

The sinusoidal dependence of supercurrent on phase as in equations 2.7 or 2.10 holds true for many junctions regardless of fabrication techniques and materials used. The cases in which the simple sinusiodal dependence breaks down have received a lot of attention. Extensive reviews of Josephson junctions that are expected to have a non-sinusoidal CPR have been written by Likharev [13] and Golubov [12].

In SIS tunnel junctions, the sinusoidal CPR is expected to hold under all circumstances. In other types of junctions, such as SNS, S-constriction-S and point-contact junctions, the CPR can be modified by a number of factors, including the electron distributions in the junction, the effects of junction geometry or the spatial distributions of the order parameter in the superconductor.

As an example, uniform, clean SNS junctions at temperatures approaching zero are expected to have a "saw-tooth" CPR given by [23]

$$I_s(\phi) = eNv_F\frac{\phi}{2} \qquad -\pi < \phi < \pi, \tag{2.12}$$

where N represents the number of conduction channels in the metal barrier and v_F is the Fermi velocity. For phase differences, $|\phi| > \pi$, outside the range given above, the CPR repeats periodically.

Another effect that can modify the CPR of any type of junction is depairing caused by large supercurrents passing through the junction. When the phase difference across this type of junction is small, the supercurrents are also small and the CPR is unchanged. However, as the supercurrent approaches its critical value,

superconductivity begins to weaken, and consequently the critical current and the phase at which the critical current is reached are both decreased. [24]

Finally, there is no reason a priori that the CPR has to be the simple sinusoidal function given by 2.7. Terms of higher order in the phase difference also satisfy the conditions presented so that the CPR could take the form:

$$j_s(\phi) = \sum_{n=1}^{\infty} j_{cn} sin(n\phi), \tag{2.13}$$

where we've replaced the total supercurrent, I_s, by the local supercurrent density, j_s, in order to emphasize that these harmonics are not due to some average behavior of the junction. The coefficients, j_{cn}, no longer represent the critical current density of the junction. Instead, the critical current is found by maximizing equation 2.13 with respect to the phase difference, ϕ.

In conventional junctions, the second-order term, j_{c2}, which corresponds to the tunneling of four electrons across the junction, is expected to be several orders of magnitude smaller than the first-order term, j_{c1}. As such, it is not expected to show a measurable effect in experiments that are sensitive to the phase of the junction. However, in both SFS and SNS π-junctions, j_{c1} goes to zero at the transition between the 0- and π-states. It has been predicted that a usually small second-order term would dominate at this transition. See for instance [25, 26, 27, 28].

Chapter 3

Superconductor–Ferromagnet Proximity Effect

3.1 Superconductor/Ferromagnetism

Several papers, both theoretical and experimental, illustrate the physics of the superconductor–ferromagnetic interaction, particularly since the realization of the first SFS π-junction [29]. For a comprehensive review of the physics, we point the reader to the work of Demler *et al.* [30] or the more recent review by Buzdin [31]. Here, we present an overview of the basic ideas contained within those and other resources.

3.1.1 Ferromagnetism

A ferromagnet has strongly coupled atomic magnetic moments that spontaneously align parallel to each other in the absence of an applied magnetic field due to an effective exchange interaction field, H_{ex}. The alignment of spins produces an energy gain, E_{ex}, that is proportional to the induced magnetization. Above a critical temperature, called the Curie temperature, spontaneous magnetization disappears because the randomizing effect of thermal fluctuations the energy gain from the ferromagnetic ordering.

Taking purely magnetostatic considerations, nearby magnetic moments will tend to align antiparallel. The internal interaction in a ferromagnet needed to overcome this classical picture is quantum mechanical in nature and results from the spin-statistics theorem.

As a simple picture, consider that the exchange interaction between two atoms, i and j, with spins, S_i and S_j, is given by the Hamiltonian [32]:

$$H = -2JS_i \cdot S_j \tag{3.1}$$

where J is the exchange integral related to the overlap of the charge distributions of the atoms i, j. When J is positive, parallel alignment of spin is obtained as a result of energy minimization.

The charge distribution of this two-electron system is dependent on the electrons' spin alignment, since the two-particle wavefunction must be antisymmetric under particle exchange. The spins will align parallel for an antisymmetric charge distribution or antiparallel for a symmetric charge distribution. From this, we can see that the difference in energy between the two different spin alignment states is the exchange energy.

3.1.2 Pair breaking

In the case of S–F bilayers, we expect that the superconducting correlations (Cooper pairs) will extend into the magnetic layer and that the ferromagnetic spin alignment will extend into the superconductor. As a result, in the interface region ferromagnetism and superconductivity coexist.

Apart from the proximity induced coexistence of ferromagnetism and superconductivity described in the previous paragraph, it is interesting to consider whether the two orders can exist in a single material. The first examples of the coexistence of antiferromagnetism and superconductivity first occured with the discovery of ternary rare-earth compounds. Other compounds have shown the onset of superconductivity at T_c followed by the onset of an inhomogeneous magnetic

order coexisting with superconductivity until at a still lower temperature the superconductivity is destroyed with the onset of first-order ferromagnetic transition.

The interaction between ferromagnetism and superconductivity was first considered by Ginzburg [33], who formulated the problem by considering an orbital mechanism by which superconductivity is suppressed (the interaction of the superconducting order parameter with the vector potential, $\mathbf{A}$, of a magnetic field).

The competition between the two states is evident from the microscopic theory of superconductivity, which makes it clear that an exchange field that tends to align spins will prevent the necessary Cooper pairing of anti-aligned spins – the so-called paramagnetic effect [34]. For the pure paramagnetic effect, the critical field, H_c – the field at which superconductivity breaks down – of a superconductor may be found from a comparison of the energy gain $\Delta E_n \sim H_c^2$ due to the electron-spin polarization in the normal state and the superconducting condensation energy $\Delta E_s \sim \Delta^2(T=0)$, where $\Delta(T)$ is the superconducting gap. From this, we see that at zero temperature the paramagnetic critical field $H_p(0) \propto \Delta(0)$.

3.1.3 Oscillation of the Cooper pair order parameter

Within the framework of the pure paramagnetic limit, Fulde and Ferrell [35] and Larkin and Ovchinnikov [36] separately predicted a non-uniform state, known now as the Fulde, Ferrell, Larkin, Ovchinnikov (FFLO) state, where Cooper pairing can still occur when the up and down electronic spin states at the Fermi energy have different momentum as in the case of the electron splitting due to the exchange interaction in a ferromagnet.

The FFLO state gives a sinusoidal modulation to the superconducting order parameter at the scale of the superconducting coherence length ξ_s. As a result, it is qualitatively different from the BCS zero-momentum state because it is spatially inhomogeneous and the order parameter contains nodes where the phase changes by π.

In the FFLO state, rather than splitting the Cooper pair state, the high energy electron gains momentum $Q \propto E_{ex}/v_F$, where E_{ex} is the ferromagnetic exchange

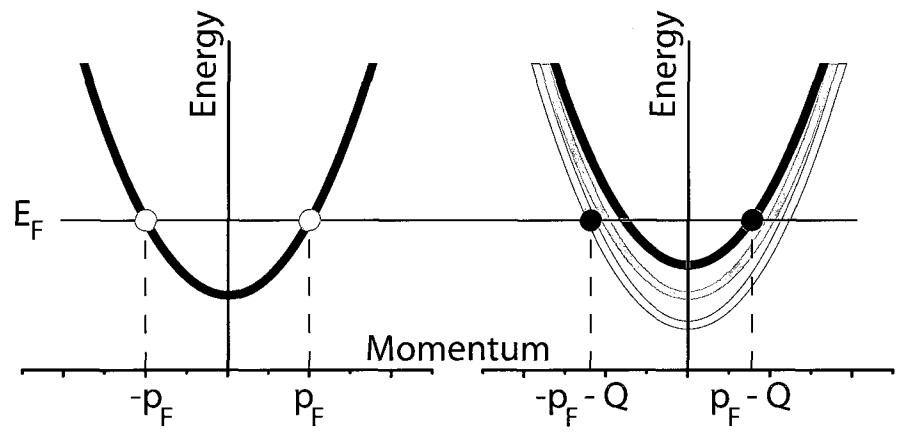

Figure 3.1: (Left) In a one-dimensional model of Cooper pairing, electrons at the Fermi surface with equal and opposite momentum, p_F and $-p_F$, form pairs (shown by red dots). (Right) In the presence of an exchange field, the spin up and spin down bands are shifted by E_{ex}. In order for Cooper pairs to form, they must pair with momentum states that are not equal, which results in a center-of-mass momentum $-2Q$ (shown with black dots) or $2Q$ (not shown).

energy and v_F is the Fermi velocity. Similarly, the lower energy electron loses momentum by the same amount, Q. This creates a total pair momentum in the ferromagnet of $2Q$. There are two states at this energy pairing, $\{Q\uparrow, -Q\downarrow\}$ and $\{Q\downarrow, -Q\uparrow\}$, and when they are added, the resulting order parameter oscillates as $cos(2Qz)$ where z is the direction of Cooper pair flow:

$$\begin{aligned} \psi(x) &= \frac{1}{2}[\psi_0 e^{(i2Qx)} + \psi_0 e^{(-i2Qx)}] \\ &= \psi_0 cos(2Qx) \end{aligned} \tag{3.2}$$

Figure 3.1 shows how the electronic energy spectrum is split into two bands with different energy and momentum states. The two terms on the right hand side of the first line of equation 3.2, represent the two equivalent pairing states with total momentum $2Q$ and $-2Q$.

This simple description of the FFLO state strictly applies only for the case of a one-dimensional superconductor. In the case of 2D or 3D superconductors, it is not possible to choose the single wave vector $2Q$ which compensates the energy splitting

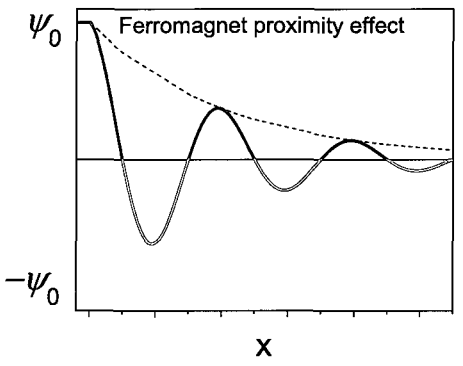

Figure 3.2: The proximity induced superconducting wavefunction in a ferromagnetic barrier (solid line) oscillates as well as decays. Where the order parameter curve is black, its phase is 0 and where it is red its phase is π. The dashed blue line shows the decaying term without oscillation that would be expected for the superconducting wavefunction in a normal metal.

for all electrons on the Fermi surface, because $2Q$ depends on the direction of v_F, and the paramagnetic limit is preserved.

3.2 SFS Josephson junctions

3.2.1 SF proximity effect

When considering the case of superconductivity induced in metallic ferromagnet, we must modify the FFLO-like picture by taking into account that the order parameter also decays on a length scale given by the normal metal coherence length, ξ_N, as was discussed in chapter 2. Thus, equation 3.2 becomes:

$$\psi(x) = \psi_0 e^{-x/\xi_N} cos(2Qx). \tag{3.3}$$

Figure 3.2 shows this oscillatory behavior compared to the usual metallic proximity effect. While in the ferromagnet, the sign changes in the order parameter due to the oscillation are equivalent to phase changes of π. From this, we expect the ability to construct a π-junction by fabricating an SFS junction such that the proximity-induced order parameter changes sign across the junction.

In practice, the qualitative FFLO-like picture works well when working with a diffusive ferromagnet. In place of ξ_N and $|\Delta p| = 2Q$, we express the decay and oscillation of the order parameter in terms of a single complex ferromagnetic coherence length, ξ_F, such that:

$$\psi(x) \propto \psi_0 e^{-x/\xi_F} + \psi_0 e^{-x/\xi_F^*}. \tag{3.4}$$

The ferromagnetic coherence length is given by [29]:

$$\xi_F = \sqrt{\frac{\hbar D}{2(\pi k_B T + iE_{ex})}}, \tag{3.5}$$

which differs from the dirty limit of the normal-metal coherence length 2.5 by the addition of the imaginary iE_{ex} term in the denominator.

Defining the real part of the ferromagnetic coherence length, ξ_{F1}, and the imaginary part, ξ_{F2}, as follows:

$$\frac{1}{\xi_F} = \frac{1}{\xi_{F1}} + \frac{i}{\xi_{F2}}, \tag{3.6}$$

we can then replace the quantities from equation 3.3 using the transformations: $\xi_N \rightarrow \xi_{F1}$ and $2Q \rightarrow (1/\xi_{F2})$. From equation 3.5 and 3.6, we derive the values of ξ_{F1} and ξ_{F2} [37]:

$$\xi_{F1} = \left\{ \frac{\hbar D}{[(\pi k_B T)^2 + E_{ex}^2]^{1/2} + \pi k_B T} \right\}^{1/2}, \tag{3.7}$$

$$\xi_{F2} = \left\{ \frac{\hbar D}{[(\pi k_B T)^2 + E_{ex}^2]^{1/2} - \pi k_B T} \right\}^{1/2}. \tag{3.8}$$

The quantities ξ_{F1} and ξ_{F2} are only equal at zero temperature or in the limit that the exchange energy is much larger that the thermal energy.

The oscillation of the order parameter in SF structures can be seen in several different types of measurements. The quasiparticle density of states at the Fermi level was predicted to oscillate in a ferromagnet in proximity to a superconductor,

enhancing at thicknesses where superconducting correlations are suppressed [38]. This effect was measured in the tunneling spectra of superconductor–ferromagnet–insulator–normal-metal tunnel junctions [39]. The tunneling spectra also make it possible to extract the magnitude of the exchange energy [40].

Also, in SF and FSF structures, the superconducting critical temperature was predicted to be non-monotonic [41] due to a boundary-matching effect [42], and verified by measurements [42, 43].

3.2.2 Oscillating order parameter and critical current

When considering the behavior of the Josephson effect in SFS junctions, we have to account for the oscillation of the order parameter in the barrier. The result is that the critical current of the junction also oscillates as a function of barrier thickness, d_F [44, 45, 46].

The prediction of the critical current oscillations in SFS junctions was first made for the clean limit [22] using the Eilenberger equations [47] and then for the dirty limit [48] by means of the Usadel equations [49]. Formal treatment of SF structures is presented in the reviews of Buzdin [31] and Golubov *et al* [12]. Instead of reproducing those formal derivations, we instead present a qualitative picture of the Josephson effect in SFS junctions by considering the overlap of the oscillating order parameters.

We consider two identical superconductors separated by a ferromagnetic layer as in figure 3.3. The finite phase difference, $\phi = \theta_L - \theta_R$, corresponds to a phase shift between the wavefunctions of the two superconductors at the interfaces:

$$\psi_L(-d/2) = \psi_0 = e^{-i\phi}\psi_R(d/2), \tag{3.9}$$

where we ignore the inverse proximity effect so that ψ_0 represents the order parameter in the superconductors far from the junction. Using equation 3.4, we can represent the order parameter in the barrier as the sum of the contributions from

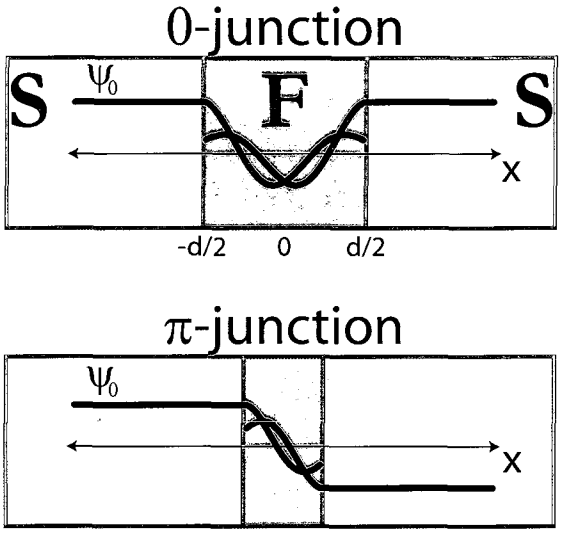

Figure 3.3: In an SFS junction, the modulation of the superconducting order parameter, ψ, can affect the ground-state energy. If the thickness of the barrier, d_F, and complex coherence length, ξ_F, are such that the oscillating term (see equation 3.10) is positive, the SFS junction behaves like a conventional 0-junction (top). However, if the oscillating term is negative, the barrier causes a ground-state phase difference of π and the junction is an unconventional π-junction (bottom).

the left and right superconductors:

$$\begin{aligned}\psi(x) &= \psi_L + \psi_R \\ &= \psi_0\Bigg[exp\left(-\frac{x+d/2}{\xi_{F1}}\right)cos\left(\frac{x+d/2}{\xi_{F2}}\right) \\ &\quad + e^{i\phi}exp\left(-\frac{x-d/2}{\xi_{F1}}\right)cos\left(\frac{x-d/2}{\xi_{F2}}\right)\Bigg].\end{aligned} \tag{3.10}$$

To get this equation, we have assumed that the barrier is sufficiently thick that $exp(-d/\xi_{F1}) \rightarrow 0$ (see [37] for the case where $d \geq \xi_{F1}, \xi_{F2}$). Substituting this equation for the order parameter into the equation for the current density in the absence of a vector potential, equation 2.2, we find the SFS current-phase relation:

$$J(d) \propto sin(\phi)\left[cos(\frac{d}{\xi_{F2}}) + \frac{\xi_{F1}}{\xi_{F2}}sin(\frac{d}{\xi_{F2}})\right]e^{-d/\xi_{F1}}. \tag{3.11}$$

Figure 3.4 shows a plot of critical current density as a function of ferromagnetic barrier thickness. The black line is the result of a fit to the data based on the

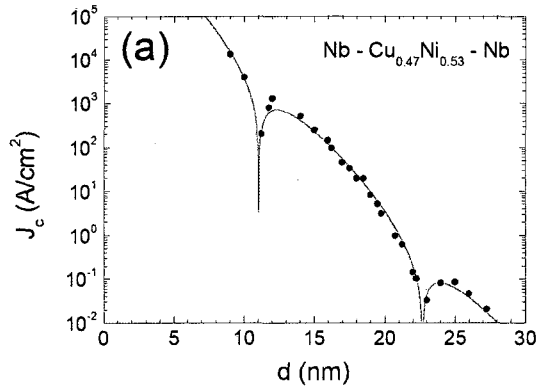

Figure 3.4: Critical current density as a function of ferromagnetic barrier thickness. The data (circles) is fit (straight line) using equation 3.11. Figure modified from [44].

equation 3.11.

Chapter 4

Niobium–Copper-Nickel–Niobium Junctions

In our research, the specific system of superconductor–ferromagnet–superconductor (SFS) Josephson junctions we use are niobium–copper-nickel–niobium (Nb-CuNi-Nb) junctions. In this chapter, we'll discuss some of the material properties of the amorphous copper-nickel films and the details of the niobium–copper-nickel interaction. We'll also discuss the techniques that have been used to fabricate these types of junctions, including a review of the older, multistep process and its weaknesses, versus the newer, improved fabrication technique used to create all of the junctions that are new to this thesis. Lastly, this chapter examines previous measurements of arrays of SFS junctions, which provide the strongest differentiation between the zero-state and the π-state.

4.1 Ferromagnetism in copper-nickel films

The choice of ferromagnet for the barrier has a significant impact on the dynamics of an SFS junction due to the dependence of the tunneling current on the strength of the exchange interaction (Equation 3.11. The four elements – nickel (Ni), cobalt (Co), iron (Fe) and gadolinium (Gd) – exhibit spontaneous ferromagnetic behavior, with Curie temperatures in the range of approximately 300K for Gd to 1400K for

Co [32]. Experiments showing critical current oscillations between the 0-state and the π-state as a function of barrier thickness have been performed on junctions made with strong ferromagnetic barriers of pure nickel (Ni), cobalt (Co), permaloy ($Ni_{80}Fe_{20}$), and iron (Fe) [50, 51, 52].

With these materials, oscillations between the 0-state to π-state occur with periods of as little as 1nm thickness variations. It is experimentally difficult to perform a careful mapping of the critical current oscillations with such small oscillation periods. The primary problems are that any barrier roughness will tend to average out the oscillations, and that precisely and repeatedly growing such thin films using traditional fabrication techniques is challenging. Experiments that have achieved success with strong-ferromagnet junctions are only able to show two to four data points per critical current oscillation period.

Diluting a strong elemental ferromagnet with either a diamagnetic or paramagnetic metal provides a means of reducing the exchange energy. Experiments using mixtures of nickel with diamagnetic copper (Cu) [29] and paramagnetic paladium (Pd) [40] have successfully shown critical current oscillations with larger periods. For the experiments in this thesis, we use junctions fabricated by the group of Valery Ryazanov at the Institute of Solid State Physics in the Russian Academy of Physics at Chernogolovka, Russia, that have niobium as both of the electrodes and barriers that are a mixture of nickel and copper (Nb–CuNi–Nb) as in [29].

The exchange interaction in iron, cobalt and nickel occurs between electrons in the partially filled 3d band with electrons in the 4s band. As a result, the bottom of the spin-up 3d subband has a lower energy than the bottom of the spin-down 3d subband. The net magnetization is then a consequence of the unequal population of these two 3d subbands. The effect is strongest in cobalt, which lies between iron and nickel on the periodic table of elements. Copper, which is to the right of nickel on the periodic table, has its 3d band fully filled and is not a ferromagnet.

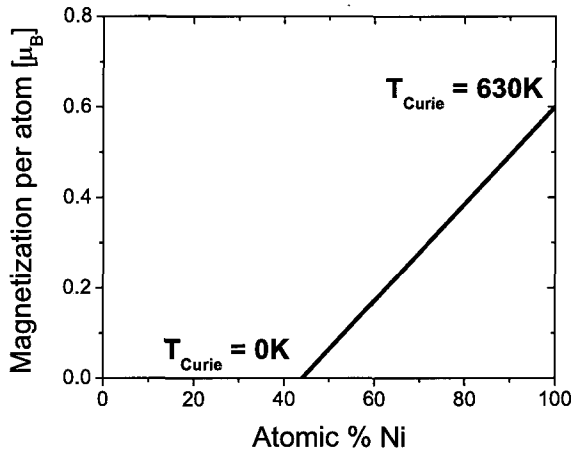

Figure 4.1: The ferromagnetic energy of $Cu_{1-x}Ni_x$ is reduced as x decreases until it no longer shows a phase transition just above x=0.4.

4.1.1 Effects of copper concentration

A qualitative understanding of the effects of copper concentration on the exchange energy of the CuNi alloy can be gained by assuming, because of their similar atomic structure, that the band structures of copper and nickel are the same. In that case, adding copper to pure nickel increases the average filling of the combined 3d band, which reduces the spin polarization and thus lowers the effective exchange interaction. Ferromagnetism is fully suppressed when the Ni concentration drops to 44% and below. Figure 4.1 shows the magnetic moment per atom in $Cu_{1-x}Ni_x$ alloys as a function of x. In pure nickel, each atom contributes $0.6\mu_B$ to the magnetization. The magnetization per atom drops linearly at a rate of $0.01\mu_B$ per atomic percent nickel. The Curie temperature also changes linearly from about 630K for pure nickel to zero at x =44% nickel.

When discussing the material properties of the thin film of CuNi that forms the weak-link of an SFS junction, it is important to consider the effects of thin-film growth. Copper and nickel are known to form uniform alloys, and both elements sputter at the same rate and with the same anisotropy. As a result, the composition of a thin film of CuNi is expected to coincide with the composition of the bulk CuNi target that was used for the film deposition. In previous work [53], Auger

spectroscopic analysis confirmed the expectation that the composition CuNi films to the bulk target from which they were sputtered contain the same level of nickel concentration.

Another concern regarding the fabrication of junctions is the interaction between the barrier material and the superconductor. Neither copper nor nickel alloy with niobium (the material we use as the superconductor), which means that the interface in Nb–CuNi–Nb multilayers should remain sharp with a narrow region of diffusion.

4.1.2 Nickel clustering

In addition to the average composition of films compared to the bulk and the diffusion of the CuNi barrier with the niobium electrodes, it is necessary to consider the microscopic composition of the CuNi films. Evidence suggests [54] that variations in thickness on the scale of 10-100 atoms may occur in CuNi films depending on the film growth conditions. Film deposition often occurs at high temperatures that allow for thermally activated mobility of the material being deposited. Atoms of nickel may tend to cluster, forming regions within a CuNi film with a higher Curie temperature.

Figure 4.2 shows the residual magnetization of a 100nm thick film of $Cu_{49}Ni_{51}$ as a function of temperature. The residual magnetization is what remains after a large coercive field is applied to the sample. Based on figure 4.1 we would expect the Curie temperature of this alloy to be approximately 160K in the bulk. In the film, we can see that the magnetization shows a quick fall-off as the temperature is increased from 2K which begins to level off around 25K, and remains finite but small up to room temperature.

An interpretation of this result is that the film is effectively composed of two parts – a uniform CuNi film with T_{Curie} of 40-60K, superimposed with nickel-rich clusters with T_{Curie} close to the value of pure nickel. Not all films measured in this way show a residual magnetization, further lending support to the claim that it is the result of variations in the fabrication process.

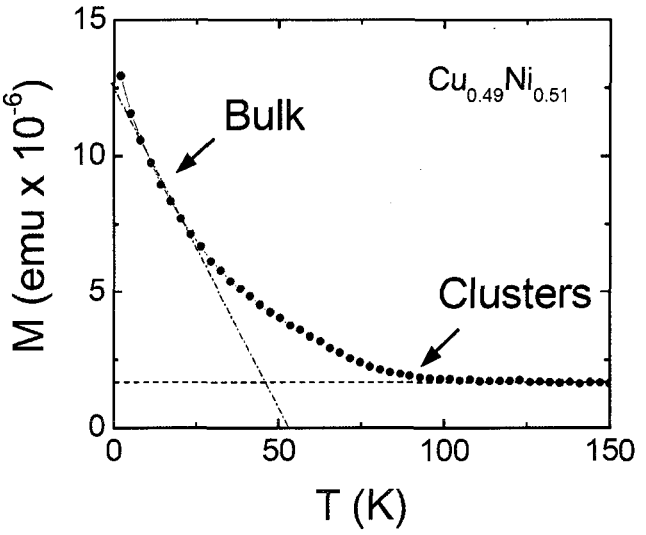

Figure 4.2: Residual magnetization of a 100nm thick film of $Cu_{49}Ni_{51}$ from [53]. The small temperature behavior is attributed to the average film magnetization, while the persistent magnetization at high temperatures is due to clusters of nickel with locally large T_{Curie}.

4.1.3 Critical current vs temperature

Another benefit of the CuNi alloy was predicted by Buzdin and Kupriyanov [41], who suggested that SFS junctions fabricated with barrier thickness, d, close to a 0-π crossover value, $d_{0\rightarrow\pi}$, can show a temperature-dependent transition.

This is possible because the real and imaginary parts of the ferromagnetic coherence length depend on temperature as well as the exchange energy (equation 3.8). In the case of SFS junctions with strong ferromagnets, the exchange energy is much larger than the thermal energy associated with the superconducting critical temperature, T_c, and we expect to be able to ignore the temperature dependence. Weak ferromagnetic barriers can have an exchange energy similar in magnitude to T_c, so we expect that changes in temperature during measurements will modulate the coherence length and thus could cause the junction to move between the 0- and π-states.

Figure 5.4 shows an example of the temperature modulation of a junction. This $I_c(T)$ dependence is much different from the conventional 0-junction behavior that was presented in figure 2.4. The first identification of the π-state of an SFS

junction by Ryazanov *et al.* [29] was based on this exotic $I_c(T)$ behavior and was reproduced by Sellier *et al.* [46] in CuNi alloys with $T_{Curie} \approx 30 - 60$K.

4.2 Junction fabrication techniques

As mentioned earlier, the junctions reported in this thesis were fabricated by the research group of Valery Ryazanov. Historically, the Ryazanov group fabricated Nb–CuNi–Nb SFS junctions with a process that required separate photolithography steps for each layer, which we refer to as the layer-by-layer method. Experimental results [54] that are reviewed in section 4.3.2 and 5.3.2 of this thesis suggested that the layer-by-layer method had a high likelihood of producing junctions with small but experimentally relevant thickness variations in the ferromagnetic barrier. The junctions in this thesis were developed using the trilayer method, a technique that does not require exposing the barrier material to air or to the chemicals used in the photolithographic process. Figure 4.3 shows a step-by-step schematic of both of these processes.

There are several benefits of using the trilayer method instead of the layer-by-layer method. When the barrier of the junction is protected, as in the trilayer process, the S–F interfaces are cleaner and result in larger current densities. Also, the barrier thickness is expected to be much more homogenous due to the significant reduction in impurities.

In addition to implementing the trilayer method, two other improvements were made to the fabrication scheme to address the proir shortcomings. First, the barrier was constructed with a thin passivating layer of copper between both of the CuNi–Nb interfaces, making the junction effectively a S–N-F-N–S junction. The additional copper layers were thin (~1nm) compared to total barrier thickness (7nm), and were designed to smooth out any thickness or exchange field variation that might occur in the CuNi layer alone.

Secondly, the junction size was reduced from 50x50μm^2 [55], 10x10μm^2 and 4x4μm^2 [54] to 5x5μm^2 and 2x2μm^2 for the junctions original to this thesis. When

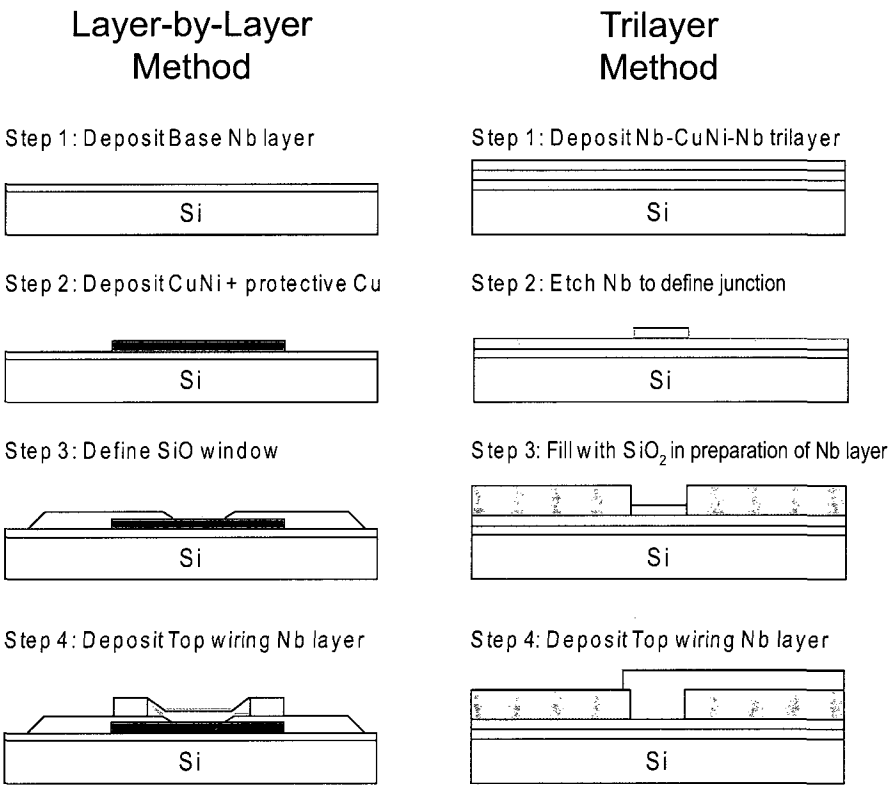

Figure 4.3: Left-hand column shows the steps used to fabricate junctions in the multilayer process. Right-hand column shows the trilayer process. The most significant difference is that in the trilayer method, the junction barrier is never exposed to air or fabrication chemicals, leading to a cleaner material.

sputtering material for thin film deposition, a cloud of material with a non-uniform spatial density is ejected from the target. Variations in density of the material over tens of nanometers at the substrate are negligably small for most junctions, but could cause concern for the effects we wish to measure.

4.3 Search for a superharmonic current-phase relation

Higher harmonics in the current phase relation of Josephson junctions, based on the perturbation arguments presented in equation 2.13 are expected to be very small [12]. In the dirty limit calculation, relevant for junctions made with a ferromagnetic alloy, the first-order terms are expected to be $j_{c1} \sim exp(-d/\xi_{F1})$ and $j_{c2} \sim exp(-2d/\xi_{F1}) \sim j_{c1}exp(-d/\xi_{F1})$. For parameters appropriate to the junctions produced by Ryazanov's group, that gives a second-order term that is as much as 10^{-4} smaller than the first-order term, making it negligible in most systems.

However, as we have seen, the first-order Josephson tunneling term vanishes as a function of thickness and temperature in SFS junctions, with the result that even a small second-order term may become dominant. In fact, shortly after the experimental realization of the 0-π transition in SFS [29] and SNS [56] junctions (which can also be modulated through the 0-π transition by quasiparticle injection), models predicting current-phase relations proportional to $\sin(2\phi)$ were proposed [57, 26, 25].

The expected signatures of a second-order tunneling term are:

(1) a non-vanishing critical current due to I_{c2} at the cusp where $I_{c1} \rightarrow 0$,

(2) frequency doubling in the magnetic field dependence of the critical current, $I_c(H)$, at the point that second-order terms become non-negligible,

(3) the appearance of Shapiro steps at half-integer values due to phase-locking to microwave excitations, and

(4) an additional zero-crossing in the current-phase relation between the phase

difference $\phi = 0$ and $\phi = \pi$.

Details of these effects will be discussed in detail in chapters 5 and 6. For now, we will discuss previous attempts to identify second-harmonics.

4.3.1 Previous results

Experiments successfully demonstrating this behavior have been claimed in both SNS [56] and SFS [46] junctions. In the case of Baselmans *et al.* [56], the field dependence of a loop containing two junctions - one near the 0-π state and the other in the conventional state - was seen to double. However, single-junction experiments on the same type of SNS junction failed to show a non-vanishing critical current term and there are known circumstances [58] under which the doubling result can occur with purely first-order junctions.

For the experiment by Sellier *et al.* [46], the appearance of half-integer Shapiro steps (3) was reported. However, experiments on SNS junctions in the conventional state have shown that microwave signals can alter the single-electron states in the barrier material, causing the appearance of half-integer steps [59] and the appearance of frequency doubling in the CPR [60].

Attempts to directly measure the CPR of SFS junctions fabricated by the Ryazanov group and measured in the Van Harlingen group [55] failed to show the expected frequency doubling (4). The junctions used were fabricated near the second thickness-dependent transition between the 0- and π-states, and it was considered likely that any second-order term would have decayed below the experimental resolution.

The first observation of the superharmonics in SFS Josephson junctions was reported by Sellier *et al.* [46], from the measurement of half-integer Shapiro steps (3) in a junction that also maintained a non-zero critical current at the 0-π crossover (1). Following that, results obtained by Frolov [54] showing both effects (1) and (3) also showed anomalous response of the junction to applied magnetic field (2). In order to reconcile the three measurements, a model based on junction inhomogeneities was proposed - the 0-π junction.

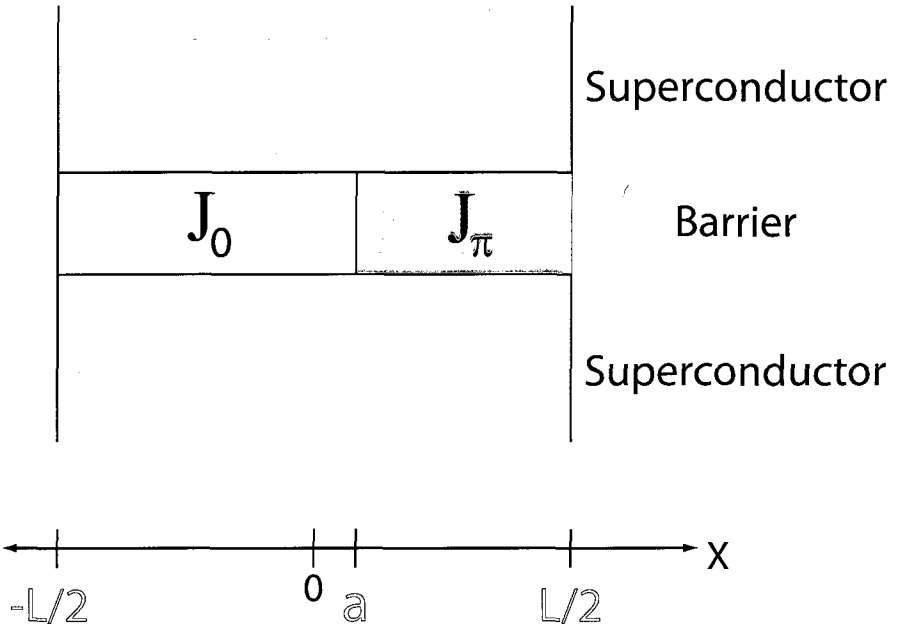

Figure 4.4: Schematic of a simple 0-π junction. Due to a small thickness variation at point a along the junction length, the two parts of the junction have different π-state crossover temperatures, $T_{\pi R} > T_{\pi L}$. In the temperature interval $T_{\pi R} > T > T_{\pi L}$, the SFS junction is partially in the 0-state and partially in the π-state .

4.3.2 0-π junction theory

A 0-π junction (different from a 0-junction or π-junction) has thickness variations across the transverse direction of the junction that may lead to sign changes in the current density [54, 61]. This effect occurs near the crossover between the 0-state and π-state. To understand this effect, consider the simplest case of a 0-π junction – a junction with one thickness step at $x = a$ as shown in figure 4.4. Because of the thickness step, the left side of the junction transitions into the π-state at a lower temperature, $T_{\pi L}$, than the right side of the junction, $T_{\pi R}$. As a result, there is a temperature, $T_{\pi R} > T > T_{\pi L}$, where one part of the junction has a current density $J_0 > 0$ while another part has current density $J_\pi < 1$.

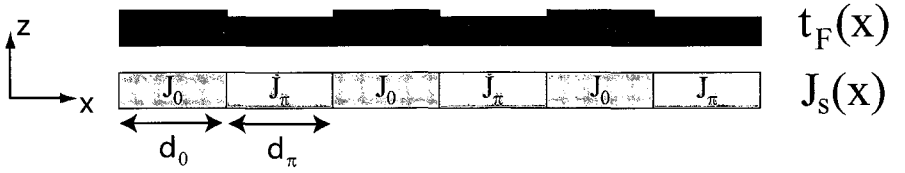

Figure 4.5: Schematic of a φ-junction barrier modeled by Mints [62] and Buzdin [66]. Variations in thickness of a ferromagnetic barrier, $t_F(x)$, shown on top gives rise to alternating 0-junction and π-junction sections with width/current density of d_0/J_0 and d_π/J_pi, respectively. Current flow is along the z-axis.

4.3.3 φ-junction theory

In principal, there could be several steps in an SFS junction as opposed to only one. Another model, first proposed by Mints [62, 63, 64, 65], can be seen as an extension of the 0-π junction into the limit of many alternating sections of 0- and π-junctions. Figure 4.5 shows the highly symmetric model of such a junction, used to calculate the expected experimental response. The direction of current flow is along the z-axis. In the transverse direction, the current density alternates in one period from J_0 to J_π with widths d_0 and d_π, respectively. The entire junction is made up of n repeated oscillations over the entire length L, where $n(d_0 + d_\pi) = L$.

In calculating the phase dynamics of this system, Mints [62] and Buzdin [66] start with the assumption, based on a mechanical analogy, that the total phase difference can be written as $\phi(x) = \varphi(x) + \xi(x)$, where φ varies slowly (on the scale of the total junction length) and ξ varies rapidly (on the length scale $d_0 + d_\pi$). Following a coarse graining approximation leads to the current-phase relation:

$$\begin{aligned} j_s &= j_\varphi + j_\xi \\ &= < j_c > (sin\varphi - \gamma sin\varphi cos\varphi) + < j_c > g(x) sin\varphi \qquad Mints \\ &= \frac{d_0 j_0 + d_\pi j_\pi}{d_0 + d_\pi} sin\varphi + \frac{-1}{\lambda_J^2} \frac{d_0^2 d_\pi^2 (j_0 - j_\pi)^2}{24|j_0|(d_0 + d_\pi)^2} sin2\varphi \qquad Buzdin \end{aligned} \tag{4.1}$$

The key information from both formulations of equation 4.1 is that the total supercurrent density has a term proportional to $sin\varphi$ with a positive coefficient, and a term proportional to $sin2\varphi$ with a *negative* coefficient ($< j_c > \gamma > 0$ in Mints' formulation). This result is in contrast to the expected *positive* second-order

coefficient resulting from the perturbation theory analysis of second-harmonics.

4.3.4 Motivating further experiments

All three models of second-order behavior – two Cooper pair events, 0-π junctions and φ-junctions – show at least some of the criteria (1)-(4). We propose that the only hope of distinguishing between these models is to measure *all four* of the criteria in a single junction. In the next two chapters, we will show in detail the physics of criteria (1)-(4). First, we show that measuring diffraction patterns and Shapiro steps can identify the positive $sin(2\phi)$ and negative $sin(2\phi)$ from the 0-π junction. Second, we will show that the direct CPR experiment (4) gives the sign of both the first-order and second-order harmonics and therefore can distinguish between the negative I_{c2} of a φ-junction and positive I_{c2} in the original perturbation argument.

Chapter 5

Transport measurements

This chapter contains explanations of the measurement techniques most commonly used to characterize all types of Josephson junctions; the I–V curve, $I_c(T)$ dependence, diffraction pattern (or $I_c(H)$ curve) and microwave excitations (Shapiro steps). The results were obtained from three superconductor-ferromagnet-superconductor (SFS) Josephson junctions fabricated with F-layer thicknesses near the first node in the $I_c(d)$ dependence.

Junctions A and B have a 5x5μm^2 area and were fabricated concurrently. They both show vanishing critical current at the 0-state to π-state crossover, Fraunhofer-like diffraction patterns and integer Shapiro steps only.

The third sample, junction C, is the smallest with a 2x2μm^2 area. It shows unconventional behavior, including non-vanishing critical current and frequency doubling of diffraction patterns near the 0-to-π crossover, as well as frequency doubling in the appearance of Shapiro steps.

5.1 Experimental setup

The experiments in this chapter involve measuring a Josephson junction in the voltage state where the current through the junction is made up of both a supercurrent component and a dissipative quasiparticle current. In order to achieve a high level of sensitivity, we exploit the large sensitivity of a dc SQUID (a

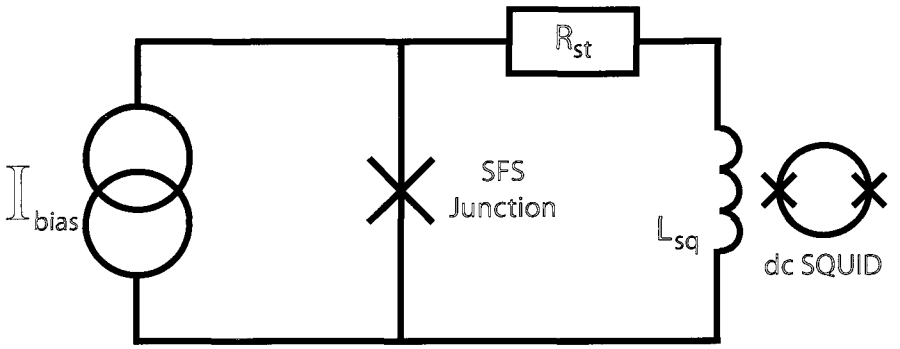

Figure 5.1: The circuit schematic for tranport measurements of Josephson junctions. The applied current divides between the junction branch and the standard resistor branch. Current through the standard resistor is converted to flux and measured by a dc-SQUID.

superconducting loop interrupted by two Josephson junctions) to magnetic flux. With a dc SQUID, one can resolve changes of as little as $10^{-8}\Phi_0$. We employ a commercial SQUID sensor manufactured by Quantum Design to measure current across its input terminals with a mutual inductance corresponding to $1\Phi_0/200nA$.

The SQUID is operated in a flux-locked loop to linearize the output, i.e. the SQUID is current-biased to a point in its V-Φ characteristic where the derivative is a minimum before ac modulation is applied. As flux is applied to the loop through the measurement leads, a modulation coil feeds in enough flux to maintain the SQUID in this optimized state. The current needed to do this is then measured as a voltage across one of several known resistors. The highest sensitivity setting has a transfer function of $0.75V/\Phi_0$.

Figure 5.1 shows a schematic of the measurement circuit with the feedback electronics for the dc SQUID excluded for simplicity. The junction is placed in parallel to L_{sq}, the inductance coupled to the SQUID. A resistor, R_{st}, in series with the inductance causes current applied across this circuit to divide between the junction and the SQUID with the transfer function:

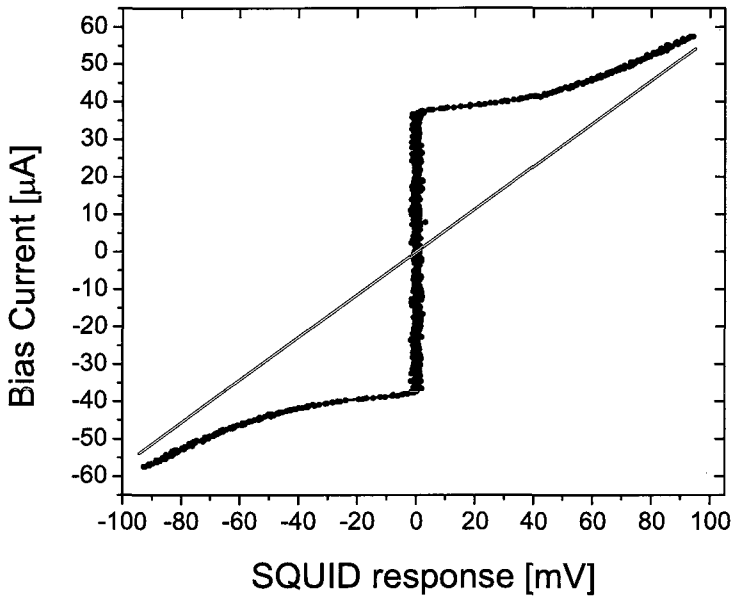

Figure 5.2: A typical I-V curve for an SFS junction with, in this case, critical current $|I_c| \approx 40\mu A$. The red curve is a guide meant to show the approximate normal state resistance of this junction.

$$\begin{aligned} V_{measured} &= \frac{0.75V}{\Phi_0}\frac{\Phi_0}{200nA}I_{sq} \\ &= (3.75mV/nA)\frac{V_{st}}{R_{st}} \\ &= \frac{3.75M\Omega}{R_{st}}V_{JJ}, \end{aligned} \tag{5.1}$$

where I_{sq} is the current through the inductance coupled to the SQUID, V_{st} is the voltage across the standard resistor, which is an equivalent voltage to V_{JJ}, the voltage across the Josephson junction. The standard resistor for our experiment approximately a strip of thin brass foil 1-5cm long. The resistance of brass is stable in the temperature range of our experiments, and the length is chosen so that R_{st} is in the range $1 - 100m\Omega$, which corresponds to a total gain in the range of $10^7 - 10^{10}$.

An example I–V characteristic is shown in figure 5.2. As the applied current is increased from zero, it all flows through the zero-resistance junction until the critical

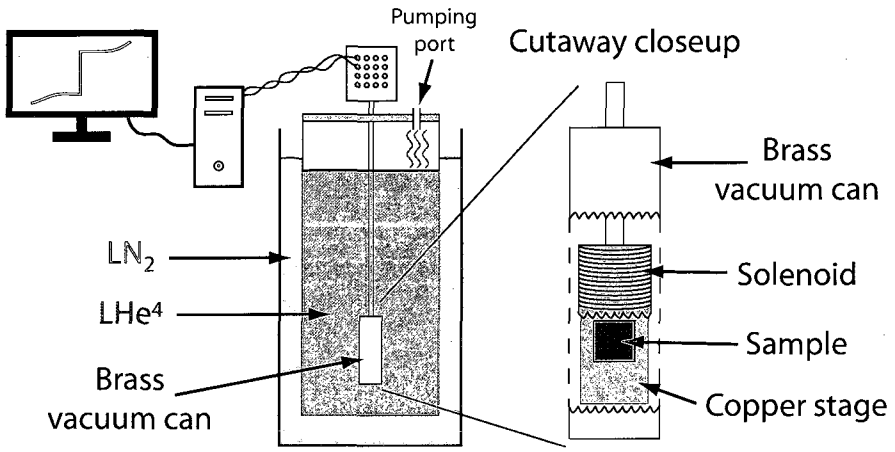

Figure 5.3: A schematic of the cryogenic probe used to measure our SFS junctions. The sample is fixed to a copper stage that is surrounded by a solenoid for applying fields. This setup is inside an evacuated brass can that provides enough thermal isolation from the cryogens that the junction can be heated. A digital to analog converter allows us to control the experiment with a computer.

current is exceeded. At that point, the junction enters the finite voltage state and the current divides between the two paths based on their relative impedances. As the bias current continues to increase, dc supercurrent flowing though the junction decreases, and the resistance approaches its normal state value, R_N.

The characteristic voltage of a Josephson junction is given by the product of the normal state resistance and the junction critical current, $V_c = I_c R_N$, and represents the largest value of V_{JJ} in a typical measurement of this type. The normal state resistance of junctions with metallic barriers is close to the resistance of the barrier which, for our ferromagnetic barriers, is $10 - 100\mu\Omega$. The maximum critical current of our junctions is about 100-300μA. Typical junction voltages are then $1 - 10$nV.

Figure 5.3 shows a schematic of the experimental setup used to make the measurements of our SFS junctions contained in this and the following chapter. The sample is fixed onto a copper stage, inside a solenoid that can be used to apply field through the junction. This staging is itself in a brass can that is sealed and pumped down to between 10^{-5} and 10^{-6} millibar, at which point we add back in a small amount of helium gas to act as a thermal exchanger. The brass vacuum can is then loaded into a dewar filled with liquid helium-4. Pumping on the helium bath

decreases its temperature through evaporative cooling to a lower limit of 1.2K. With this configuration, we can achieve sample temperatures from ~1.2K up to ~15K.

For these transport measurements, the temperature was measured from a calibrated resistor that is read out by a Lakeshore 330 temperature bridge. The resistor was affixed to the opposite side of the copper stage from the sample so that the thermal difference between them is small when the system is given time (typically 1-2 minutes) to equilibrate. Based on the calibration curve, the minimum error expected in the temperature readout is approximate 1-2mK. Accounting for thermal lag, it is expected that the actual error in the reported temperature is less than 5mK. Throughout this chapter, most of the quoted temperature values were recorded after allowing the system to equilibrate for several minutes using the built in feedback controls to set the temperature.

5.2 Critical current vs Temperature

For SFS junctions with a barrier thickness more than 1-2nm from a thickness dependent 0-to-π transition, the critical current of the junction increases monotonically with decreasing temperature as expected for a conventional Josephson junction. However, in the narrow range of $\pm$1nm from a thickness dependent transition, the temperature dependent critical current shows a node indicative of the 0-to-π transition as shown in figure 5.4.

Junctions A, B and C were all prepared near the first node of $I_c(d)$, where the critical current density changes by approximately $50 - 100(A/cm^2)/K$. The rate is much lower near the second node, only about $0.1(A/cm^2)/K$. It is not possible to observe two temperature-driven 0-π transitions in one junction. The change in effective barrier thickness due to the change in the order parameter oscillation period in the temperature interval from 0K to 10K is on the order of 1nm, whereas a change in thickness on the order of 10nm separates the nodes of the $I_c(d)$ dependence. See chapter 4 for more details.

The π-state of an SFS Josephson junction was first identified through the

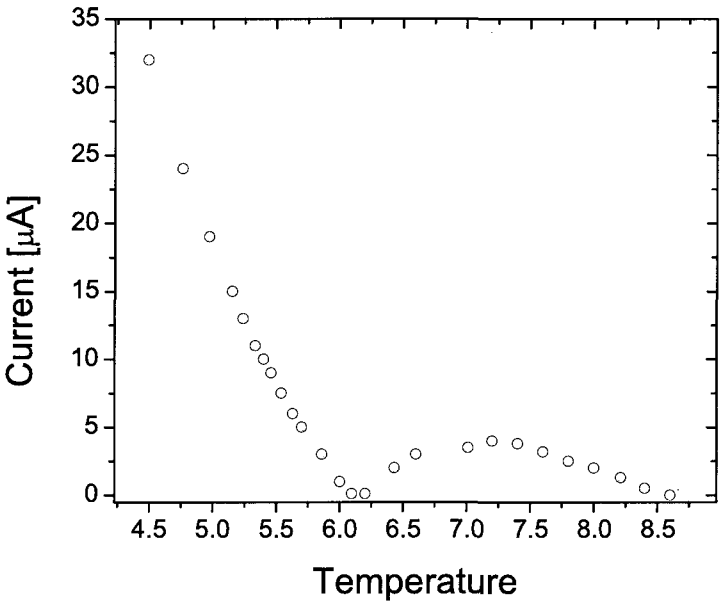

Figure 5.4: Critical current as a function of temperature for junction A – a 5x5 μm^2 trilayer SFS junction. The oscillation length is weakly temperature dependent, so the junction can be made to transition from the 0-state to the π-state.

temperature dependence of the critical current [29], which is much different in this type of junction than in a conventional junction (figure 2.4).

5.2.1 Vanishing I_c

In the case that there is no second-order tunneling term, we expect that the critical current of our SFS junctions will reach a minimum value of $I_c = 0$ at a temperature, $T < T_c$ as observed in figures 5.4 and 5.5. Both junctions A and B show this vanishing effect. There are two possible explanations for this zero value. The simplest is the case of a spatially uniform junction. Then, the temperature at which the junction reaches a critical current of zero represents the crossover temperature between the 0-state and the π-state, T_π.

Behavior similar to that shown in figure 5.4 and 5.5 has also been observed in SFS junctions with spatially non-uniform barriers. This is the case of the 0-π junction discussed in chapter 4. To see how the critical current cancels for a 0-π

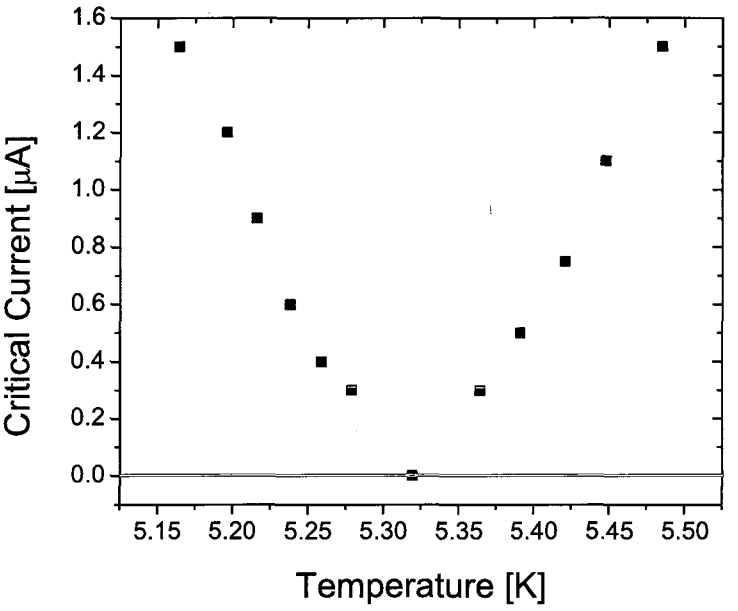

Figure 5.5: Critical current as a function of temperature for junction B showing a node at the 0-to-π transition temperature, T_π.

junction, we consider again the case of a junction with two sections of different ferromagnetic layer thicknesses. We expect the two sections to have different crossover temperatures corresponding to their different thicknesses. Despite having different 0-to-π crossover points, the junction only achieves a net zero critical current at one temperature. The total critical current of the junction decreases as both sections approach their crossover temperatures. Once one section crosses T_π, its critical current becomes negative and increases monotonically. The total junction critical current continues to shrink until the negative critical current of the thin part and the positive critical current of the thicker part exactly cancel each other. Below this $T_{0-\pi}$ temperature, the total critical current of the junction is finite and negative.

5.2.2 Non-vanishing I_c

Junction non-uniformity as described in the previous section can also lead to a non-vanishing temperature-dependent critical current as in figure 5.6 if the junction is in a regime where spontaneous currents circulate between adjacent 0- and π-state

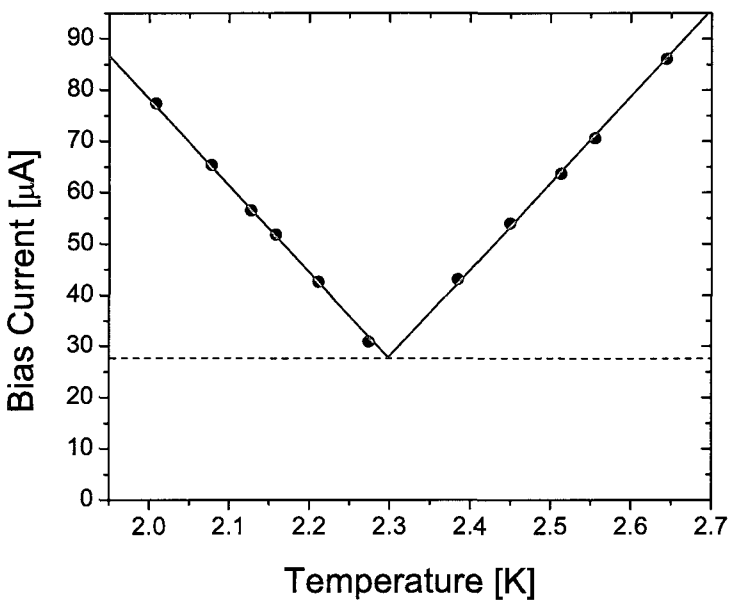

Figure 5.6: Critical current as a function of temperature for junction C, a 2x2μm^2 trilayer SFS junction where the critical current at the transition temperature remains finite. The dashed red line marks the minimum value of 27.7μA based on the linear fit shown in blue. The analytic equation for the fit is $I_c(T) = 27.7\mu A + (169.1\mu A/K)|T - (2.30K)|$.

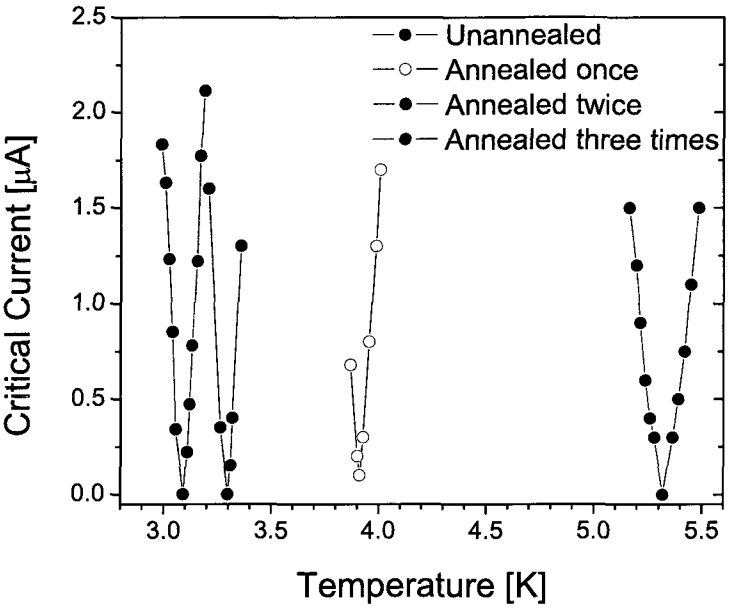

Figure 5.7: T_π shifts lower as a result of annealing the junction barrier. Each time junction B was annealed, the amount by which the crossover temperature changed, ΔT_π, decreased. In other words, the exchange energy lowering process became less sensitive to the annealing process.

sections of the junction [54].

An alternative explanation for the non-vanishing critical current is that the junction contains higher harmonics in the current-phase relation. In chapter 4, we derived the second-harmonic term due to the φ-junction model and found that it is expected to be negative and large compared to the local four-electron tunneling model.

To determine the cause of the non-vanishing $I_c(T)$ result shown by junction C, we need to distinguish between the 0-π junction model from the two $sin(2\phi)$ models. This can be done by measuring the magnetic field response of the junction.

5.2.3 Annealing

In chapter 4, we showed that copper-nickel films can exhibit a persistent magnetization well above the expected Curie temperature for the bulk CuNi

mixture (figure 4.2). We argued that the effect was caused by clustering of Ni atoms into islands that had a large local magnetization and Curie temperature. The clustering also reduces the average exchange energy of the bulk of the film.

In our SFS junctions, annealing at temperatures around 90 °C caused the zero of the critical current to shift to a lower temperature. A decrease in T_π suggests that the barrier exchange field decreased, and can also be explained by Ni clustering.

Figure 5.7 shows several $I_c(T)$ curves taken after successive annealing procedures. Each time, the sample was heated to 90 °C in an oven for 15 minutes. After the first annealing procedure, the value of T_π decreased by ~1.4K. The following two annealing processes only lowered T_π by a total of ~0.8K. The substantial differences in ΔT_π indicates that the exchange interaction lowering process becomes less thermally active. In terms of Ni clustering, this would indicated that the islands of Ni reach a maximum size.

Annealing of these junctions could be responsible for the type of ferromagnetic barrier non-uniformities described by the 0-π junction or for the more subtle non-uniformity described by Mints [62] and Buzdin [66]. If that is the case, annealing of junction B did not cause enough of a barrier spatial variation to transition from the small inhomogeneity limit to the large inhomogeneity limit [54] that would result in a non-vanishing critical current at the minimum $I_c(T)$ value.

Junctions fabricated at the first node in the $I_c(d)$ dependence are sensitive enough to changes in barrier exchange energy that they show the annealing effects even if the sample temperature is never raised above room temperature. Figure 5.8 shows two $I_c(T)$ curves for junction C measured approximately 11 months apart. The temperature of zero critical current has shifted by $\approx$ 0.07K. In junctions previously measured by the Van Harlingen group [53], T_π shifted by ~0.25K in as little as two months.

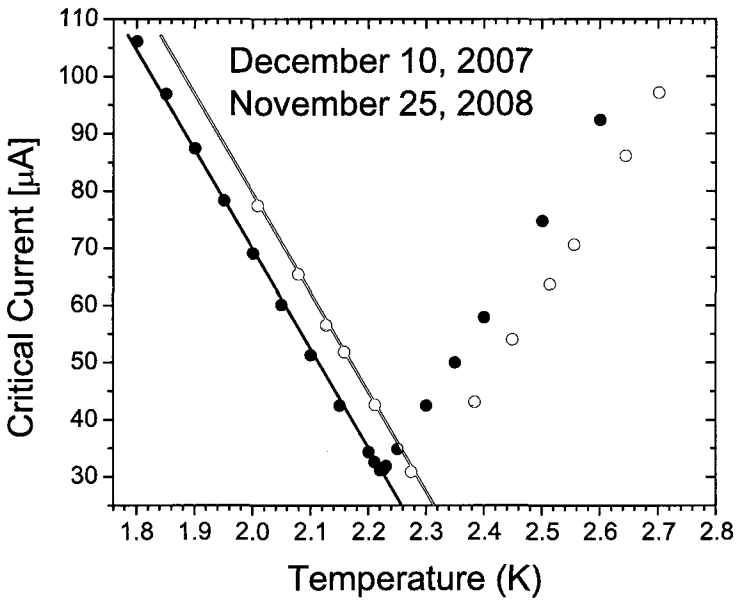

Figure 5.8: Two $I_c(T)$ curves taken 11 months apart which show the effect of room-temperature annealing on the location of T_π. The difference is $\Delta T_\pi \approx 0.07K$. The solid lines are meant to emphasize the difference in current for a given temperature.

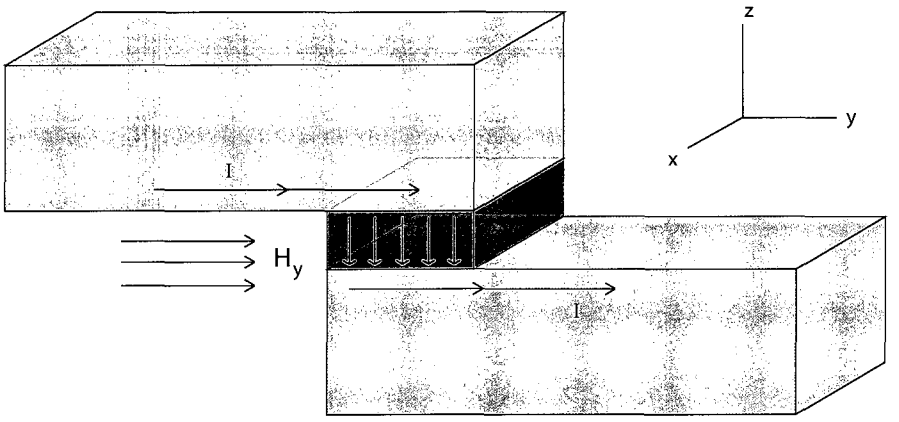

Figure 5.9: A schematic of the junction diffraction measurement. The current travels through the superconductors (pink) within a penetration depth of the edge. In the short junction limit, the current through the junction (green) passes uniformly through the whole junction area.

5.3 Critical current vs external field

Applying magnetic fields through a Josephson junction modulates the critical current of the junction by creating a gradient in the phase of the superconducting order parameter transverse to the direction of current flow [67]. By studying this modulation, we can gain information both about the current-phase relation of the junction and about any non-uniformities in the junction critical current.

For small junctions[1] where self-fields (magnetic fields generated by current passing through the junction) can be neglected, the phase of the junction in a uniform applied field is given by:

$$\phi(x) = \frac{2\pi d}{\Phi_0} H_y x + \phi_0, \tag{5.2}$$

where current flow is assumed to be along the z-axis, and the applied field, H_y, is assumed to lie along the y-axis so that the phase gradient is entirely along the x-axis. Also, $d = 2\lambda + t$, is the magnetic thickness of the junction given by the sum of the barrier thickness, t, and the magnetic penetration depth, λ, into the

[1]Small junctions are defined as junctions for which the transverse dimensions are smaller than the Josephson penetration depth, $L < \lambda_J = \left(\frac{\hbar}{2e\mu_0 d J_c}\right)^{1/2}$, which is the distance over which screening currents flow in the junction.

superconductors on either side of the barrier (for all of our junctions, we assume $\lambda_1 = \lambda_2 = \lambda$ since both superconducting electrodes are the same material). See Figure 5.9 for a schematic of the measurement.

In the conventional case of first-order Josephson tunneling, the critical current density through the junction is given from equation 5.2 by,

$$\begin{aligned} J(x) &= J_c sin(\phi(x)) \\ &= J_c sin\left(\frac{2\pi d}{\Phi_0} H_y x + \phi_0\right), \end{aligned} \tag{5.3}$$

and the total current is found by integrating:

$$I = \iint dx dy J_c(x,y) sin\left(\frac{2\pi d}{\Phi_0} H_y x + \phi_0\right), \tag{5.4}$$

where we've written $J_c \equiv J_c(x,y)$ to allow for spatial variations due to sources other than applied magnetic field, e.g. barrier thickness variations.

Rewriting this expression in complex notation and maximizing with respect to the arbitrary phase factor ϕ_0 gives:

$$I(k) = \left| \int_{-L/2}^{L/2} dx I(x) e^{ikx} \right|, \tag{5.5}$$

where $k = 2\pi d H_y/\Phi_0$, L is the length of the junction along the x-axis and $I(x) = \int dy J_c(x,y)$.

If we assume no variation in the current density of a square junction, then integration of equation 5.5 yields

$$I(\Phi/\Phi_0) = I_c \left| \frac{sin\left(\frac{\pi\Phi}{\Phi_0}\right)}{\left(\frac{\pi\Phi}{\Phi_0}\right)} \right|, \tag{5.6}$$

which is the traditional Fraunhofer pattern analogous to the diffraction of light from a single slit. I_c is the zero-field critical current of the junction, and $\Phi = H_y L d$ is the magnetic flux through the junction.

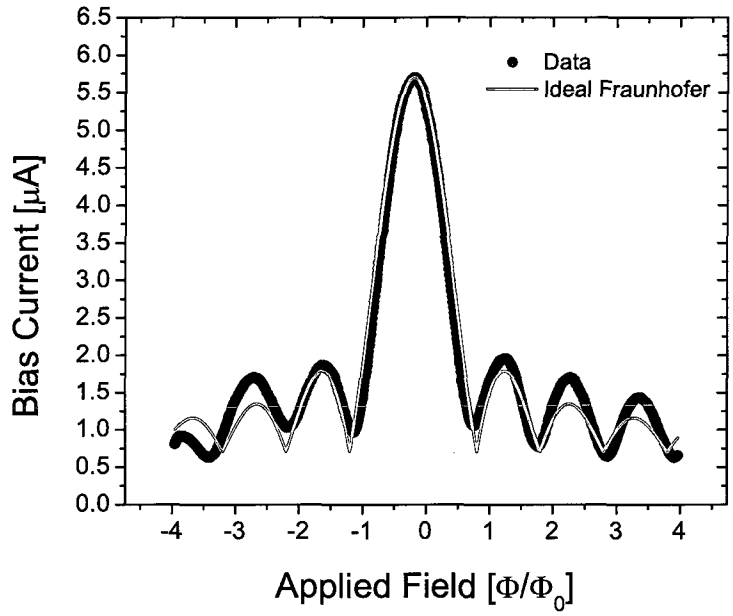

Figure 5.10: The black data points show the diffraction pattern of junction B (same junction as Figure 5.5), which is a nearly Fraunhofer response to applied field. The red curve was generated by hand from equation 5.6 to match the data as close as possible.

5.3.1 Measuring diffraction curves

Figure 5.10 shows data taken on sample B with a fit-by-hand Fraunhofer curve in red. Two reasons that the data doesn't exactly match a Fraunhofer pattern are the following:

First, the position of I_c^{max} is offset from zero field. This can be due to self-field effects if the junction *cannot* be described by the "short"-junction limit. Alternatively, there can be a magnetic field background that is causing an offset to the applied field from our solenoid. In the former case, the diffraction pattern obeys inversion symmetry, i.e. $I_c(I,H) = I_c(-I,-H)$, whereas the latter case is symmetric about the current alone, i.e. $I_c(I,H) = I_c(-I,H)$.

When testing for self-field effects by reversing the polarity of the applied current bias, we have never seen inversion symmetry. In addition, all the junctions we've measured have their expected Josephson penetration length $\lambda_J \geq 2.5L$ which

is large enough that the short-junction limit applies.

The second non-Fraunhofer feature is that the measured current never reaches zero. One explanation is based on the fact that the measurment technique we use is not a true measurement of the junction critical current. Instead, we use a feedback technique to maintain the junction in its finite voltage state at some small but non-zero value of voltage. The computer operated current supply uses a PID (proportional, integral, differential) feedback technique whereby the junction voltage is compared to a setpoint and the bias current is adjusted up or down in order to match the real voltage to the setpoint voltage.

When the junction critical current is large, the bias current and actual critical current are very close. However, the bias current must always be non-zero to reach a finite voltage, so at low values of critical current, e.g. when the applied flux $\Phi = \Phi_0$, the true critical current and the bias current differ by as much as V_{bias}/R_N, where R_N is the normal state resistance.

Despite its limitations, the PID technique allows us to measure a single diffraction pattern containing thousands of magnetic field steps in a short amount of time. Our goal is to compare the measured $I_c(H)$ curve to the models of the junction CPR that we have developed. Both junction A and junction B had $I_c(H)$ dependences like the one shown in 5.10 at all temperatures – consistent with the theoretical result for a spatially uniform junction with first-harmonics only in its CPR.

5.3.2 Non-uniform current density: 0-π junctions

In order to consider the effects of non-uniformities in the junction current density, we return to equations 5.5 and 5.4. In the non-uniform junction, $J(x, y)$ cannot be assumed constant.

The supercurrent density non-uniformities we consider are from spatial variations leading to 0-π junction. As a reminder, the 0-π junction is an SFS junction with some number of thickness steps in the ferromagnetic layer that each have slightly different 0-to-π state crossover temperatures. Far from these

temperatures, the entire junction is either in the 0-state or the π-state, and the critical current density is approximately constant – the junction returns to the uniform Josephson junction picture.

Near the 0-to-π crossover, however, a different picture emerges. The variation in T_π across the width of the junction means that the junction is in the mixed 0-π state containing both positive and negative current densities. Consider the simplest such junction with width L along the x-axis. If a single step exists at position a, the current density would be:

$$J(x) = \begin{cases} J_0 & -L/2 < x < a, \\ J_\pi & a < x < L/2, \\ 0 & |x| > L/2, \end{cases} \tag{5.7}$$

where a is the point in the interval $-L/2 < a < L/2$ at which the barrier changes thickness. Also, J_0 is and positive while J_π is negative.

This type of current density variation leads to an $I_c(H)$ dependence that is reminiscent of a d-wave SQUID [68] which shows a dip at zero-field in its $I_c(H)$ curve. Figure 5.11 shows previous measurements [54] on a non-uniform SFS junction. The schematic at the top shows the spatial non-uniformity used to generate the simulated curves.

None of the junctions A, B or C that we measured showed this type of behavior. Junctions A and B did not develop a zero-flux dip even after annealing to their lowest T_π values. This provides strong evidence that any spatial non-uniformities that may exist in the three junctions we measured cannot be modeled in terms of the simple 0-π junction.

5.3.3 Diffraction of a $sin(2\phi)$ junction

Figure 5.12 shows diffraction patterns of junction C at four different temperatures around its transition temperature.

In order to understand the frequency doubling of peaks that occurs in figure

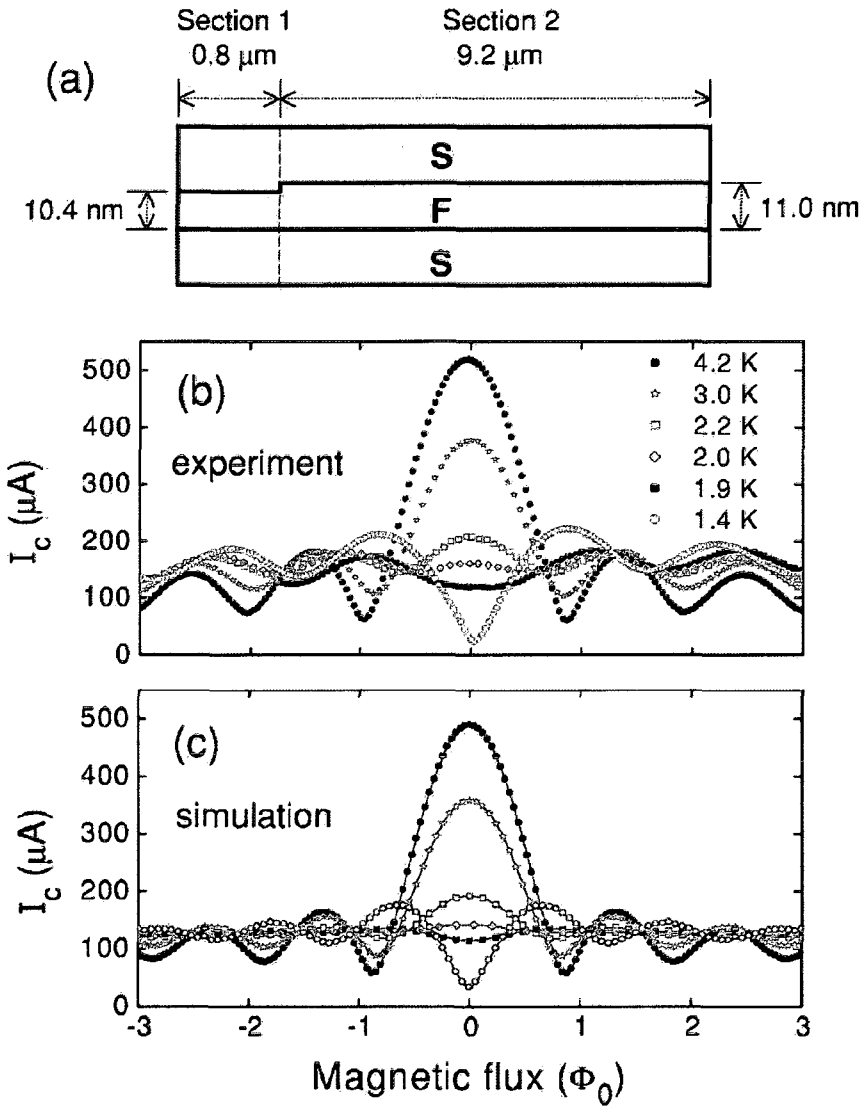

Figure 5.11: (a) Theoretical shape of the spatial non-uniformity in an SFS junction that was needed to aquire the best fit of the simulated curves (c) to the real data (b). Reprinted figure with permission from [54]. Copyrighted (2006) by the American Physical Society.

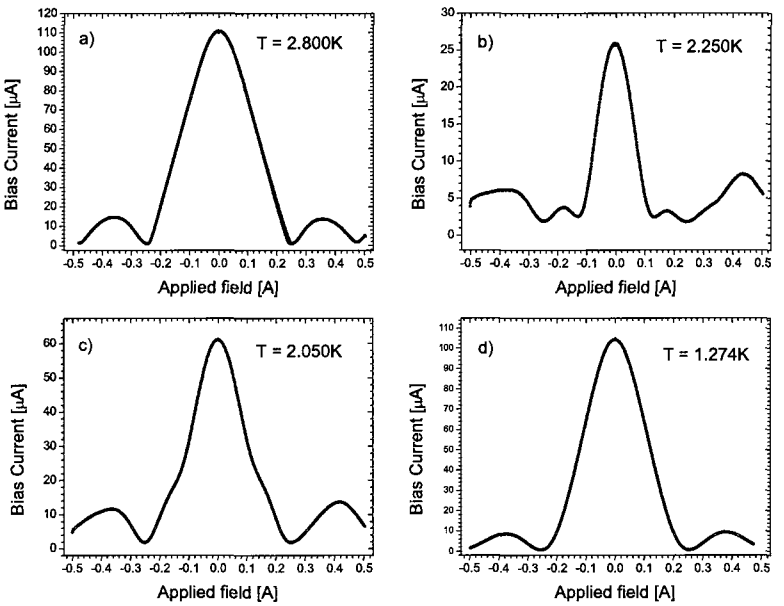

Figure 5.12: A series of diffraction patterns at different temperatures. Part a) shows a Fraunhoffer-like pattern at 2.800K - approximately 0.2K above T_π. Part b) shows the diffraction pattern very close to the crossover temperature, where the first $I_c(H)$ minimum occurs at half the field of the minimum in part a). Parts c) and d) are at still lower temperatures showing the disappearance of the doubling as I_{c2}/I_{c1} decreases.

5.12(b), we should consider the theoretical $I_c(H)$ dependence assuming the CPR can be described in terms of first- and second-harmonics.

We must return to equation 5.3, which becomes

$$J(x) = J_{c1} sin\left(kx + \phi_0\right) + J_{c2} sin\left(2kx + 2\phi_0\right), \tag{5.8}$$

where we're using $k = 2\pi d H_y/\Phi_0$ as originally defined in equation 5.5.

Following the derivation of Goldobin *et al.* [69], we do not switch to complex notation. We do assume that the critical current density is uniform across the junction width. For the φ-junction, it is still valid to assume that the current density is uniform because the non-uniformity has already been taken into account in the CPR.

The current through the junction is given by integrating equation 5.8:

$$\begin{aligned} I(k,\phi_0) &= W\int_{-L/2}^{L/2} dx\left[J_{c1} sin(kx+\phi_0) + J_{c2} sin(2kx+2\phi_0)\right] \\ &= W\int_{-L/2}^{L/2} dx[J_{c1}(sin(kx)cos(\phi_0) + cos(kx)sin(\phi_0)) \\ &\qquad + \quad J_{c2}(sin(2kx)cos(2\phi_0) + cos(2kx)sin(2\phi_0))] \\ &= W\left[\frac{2}{k}J_{c1} sin(kL/2)sin(\phi_0) + \frac{1}{k}sin(kL)sin(2\phi_0)\right] \\ &= \frac{I_{c1} sin(\pi\Phi/\Phi_0)sin(\phi_0)}{\pi\Phi/\Phi_0} + \frac{I_{c2} sin(2\pi\Phi/\Phi_0)sin(2\phi_0)}{2\pi\Phi/\Phi_0}. \end{aligned} \tag{5.9}$$

To find the the actual $I_c(H)$ dependence from this equation, we maximize with respect to ϕ_0 by calculating $\partial I/\partial\phi_0 = 0$. The two solutions for ϕ_0^{max} are phases $\phi_\pm$ defined by:

$$cos(\phi_\pm) = \frac{-I_{c1} \pm \sqrt{I_{c1}^2 + 32 I_{c2}^2 cos^2(\pi\Phi/\Phi_0)}}{8 I_{c2} cos(\pi\Phi/\Phi_0)}. \tag{5.10}$$

To determine the correct choice for $\phi_0 = \phi_\pm$, we must consider their effect on the physical system. If I_{c1} and I_{c2} have the same sign, then the positive solution of this equation, corresponding to ϕ_+, is valid for all magnitudes of $I_{c1,2}$ and fields, $k(H)$. It is also the solution for conventional Josephson junctions in the limit that

$I_{c2} \rightarrow 0$. The negative solution, however, is valid only for $|\frac{I_{c2}}{I_{c2}}| > 0.5$ and then only for certain values of the field. It always produces a smaller critical current than the critical current given by using the positive solution.

On the other hand, if I_{c1} and I_{c2} have opposite signs, then the valid solution is the negative case, ϕ_-, and the positive case is the solution with limited applicability.

This equation does not distinguish between the relative signs of I_{c1} and I_{c2}, so it cannot help us determine the mechanism (4e-model or φ-junction model) that is responsible for the second-harmonic CPR dependence.

5.4 Shapiro steps

The coupling of microwaves to the ac Josephson current density is often used to infer the general behavior of the CPR (see for example [46, 28]).

In the usual I-V measurement as shown in figure 5.2, there is a zero voltage supercurrent plus the resistive state approaching the normal state resistance. In the voltage state, the phase across the junction winds according to the differential equation

$$\frac{\partial \phi}{\partial t} = \frac{2eV}{\hbar} \tag{5.11}$$

Integrating this equation, we get the time dependent phase, $\phi = \phi_0 + (2e/h)Vt$. Plugging back into the current-phase relation of the junction, we get the ac Josephson effect

$$J = J_c sin(\phi_0 + \frac{2e}{h}Vt) \tag{5.12}$$

Applying an ac voltage to a junction in the resistive state produces resonances at voltages corresponding to the frequency of the applied excitation.

$$V_n = \frac{hn}{2e}f \tag{5.13}$$

We can see that this is true by considering a junction in the short junction limit with an uniform alternating electric field across the junction produced from an

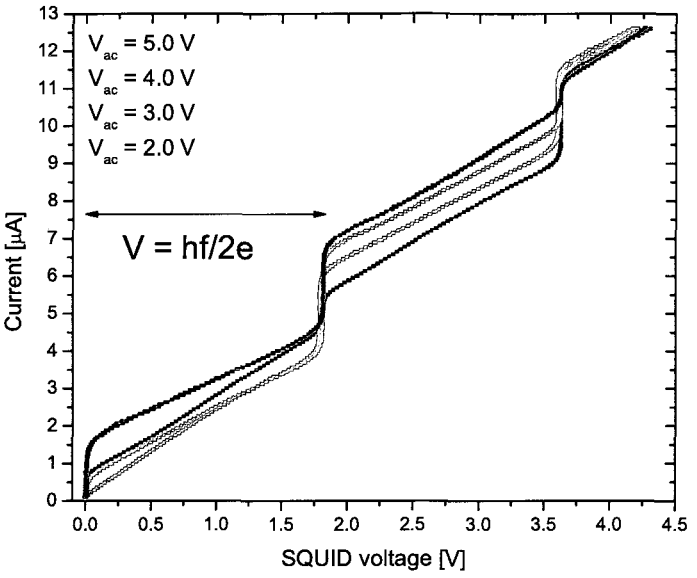

Figure 5.13: Shapiro steps for junction A as four excitation voltages. Steps appear at integer values of n.

ac voltage source. We'll also assume that the current density is uniform over the sample. In this case, the applied voltage across the junction is $V(t) = V_0 + V_{rf}\cos(2\pi ft)$, which we integrate to find the induced phase difference across the junction

$$\phi(t) = \frac{2eV_0}{\hbar}t + \frac{2e}{\omega_a\hbar}V_{rf}\sin(2\pi ft) + \phi_0. \tag{5.14}$$

The current is then given from the usual Josephson relation by $J(t) = J_c\sin(\phi(t))$. Expanding this produces a current which is a sum of Bessel functions. Upon time averaging, we see that the ac parts of the sum cancel whenever the voltage across the junction matches the applied frequency as shown in equation 5.13. This results in sharp steps in the I–V characteristic, which are called Shapiro steps [70].

Figure 5.13 shows the Shapiro step response of junction B to four different applied ac voltages. The curves only show steps at integer values of the relation 5.13. This agrees with the interpretation from $I_c(T)$ and $I_c(H)$ that the CPR of

these junctions contains only first-order harmonics.

5.4.1 Half-integer steps: 0-π junctions

In 0-π junctions that contain spontaneous currents, half-integer Shapiro steps were observed at temperatures near the $T_{0-\pi}$ point [54]. In this type of junction, half-integer steps occured only over a small temperature range ($\pm 35mK$) in which the junction is expected to be in the non-uniform phase state.

Figure 5.14 shows the maximum Shapiro step height as a function of temperature for the $n = 1/2$ and $n = 1$ steps in a 0-π junction.

To explain the presence of half-integer steps in the case of a 0-π junction, Frolov again draws an analogy to the 0-π SQUID [68, 54].

5.4.2 Half-integer steps: the $sin(2\phi)$ junction

To derive the result of microwave excitation in the case of second-order tunneling, we can follow the same procedure in the case of the conventional junction where the time varying current density is expanded in terms of Bessel functions. Once that is done, the time-averaged current density is found to be:

$$\overline{j_s(A,\phi_0)_n} = \left| j_{c1}\sin(\phi_0)\mathrm{J}_n(A) + j_{c2}\sin(2\phi_0)\mathrm{J}_{2n}(2A) \right|, \tag{5.15}$$

where A is the amplitude of the phase oscillations ($\phi = \phi_0 + \omega_J t + Asin(2\pi f t)$) and J_n and J_{2n} are the integer-type Bessel functions [69]. The amplitude of the steps correspond to the maximum of the supercurrent with respect to ϕ_0, which occurs for

$$cos(\phi_0) = \frac{-j_{c1}\mathrm{J}_n(A) \pm \sqrt{(j_{c1}\mathrm{J}_n)^2(A) + 32j_{c2}^2\mathrm{J}_{2n}^2(2A)}}{8j_{c2}\mathrm{J}_{2n}^2(2A)}. \tag{5.16}$$

Substituting this equation in yields a rather unwieldy expression for the amplitude of the steps and is not shown here. In the case of the half-integer steps, we can examine the $sin(2\phi_0)$ term alone, so the expression for the time-averaged

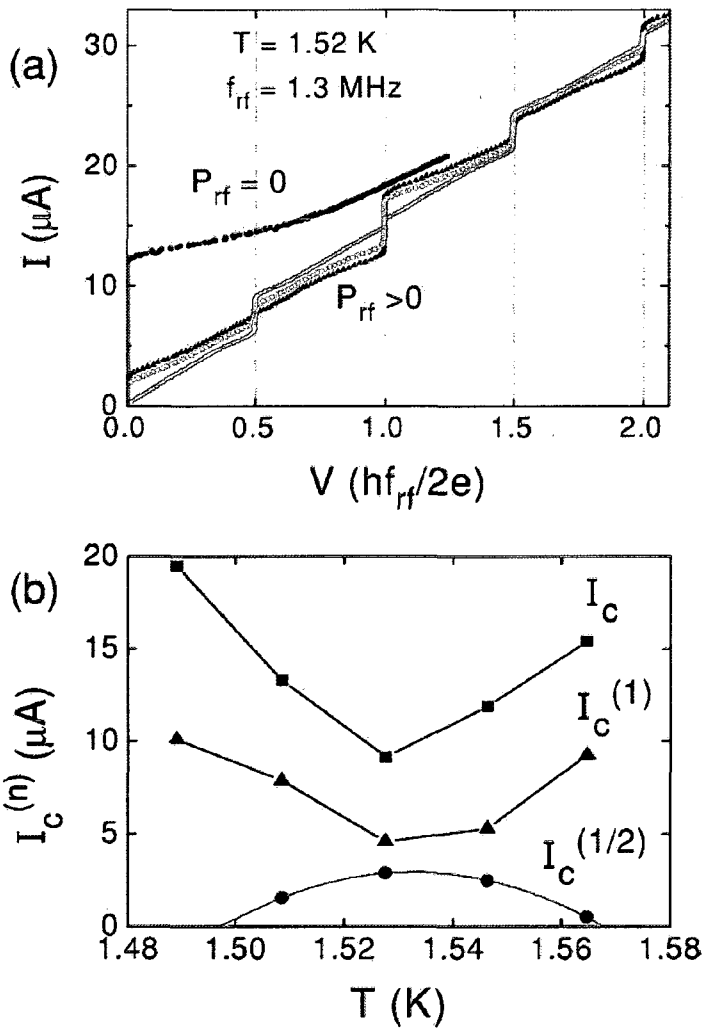

Figure 5.14: Shapiro steps for a 0-π junction appear in the top panel at a temperature, $T = 1.52K$ close to the temperature at which $I_c(T)$ is minimized. Panel (b) shows the maximum current step for the n=0, n=1/2 and n=1 steps showing the dome shape characteristic of half-integer Shapiro steps in a 0-π junction. Reprinted figure with permission from [54]. Copyrighted (2006) by the American Physical Society.

current density is:

$$\overline{j_s(A,\phi_0)_n} = j_{c2} sin(2\phi_0) \mathrm{J}_{2n}(2A) \quad (5.17)$$

$$j_s^{max}(A,\phi_0)_n = |j_{c2} \mathrm{J}_{2n}(2A)| . \quad (5.18)$$

It is clear that half-integer Shapiro steps should appear in the characteristic of a junction as long as $j_{c2} \neq 0$. Also, the relative sign of the first- and second-order tunneling currents cannot be distinguished from this measurement.

A calculation by Moshe and Mints [71] claimed that the relative sign of j_{c1} and j_{c2} could be determined in the case that a magnetic field is applied to the junction while measuring Shapiro steps. In this case, the damping was not taken into account, so it's direct application to experimental analysis is questionable.

5.4.3 Measurement of half-integer steps

Measuring Shapiro steps can be technically difficult. Using equation 5.13, we can predict at what junction voltage half-integer and integer steps should occur for a given excitation frequency. In our measurement setup, we measure the amplified dc SQUID voltage V_{sq}, which has the transfer function given in equation 5.1. The small resistances we use for R_{st} to optimize the readout means that any extra resistance in the wiring can cause a non-negligable change in the SQUID voltage value for a given junction voltage.

In the case of stray resistance, we replace R_{st} in equation 5.1 with $R_{eff} = R_{stray} + R_{st}$. Then the location of steps is given by:

$$V_n = \frac{R_{eff}}{3.75 M\Omega} \frac{nh}{2e} f_{rf}. \quad (5.19)$$

R_{eff} must be less than $1.5R_{st}$ (50% larger than the expected value of R_{st}) if we hope to identify persistent half-integer Shapiro steps.

Another way to identify the presence of half-integer steps is to observe the voltage separation between steps decrease by a factor of two. For example, at

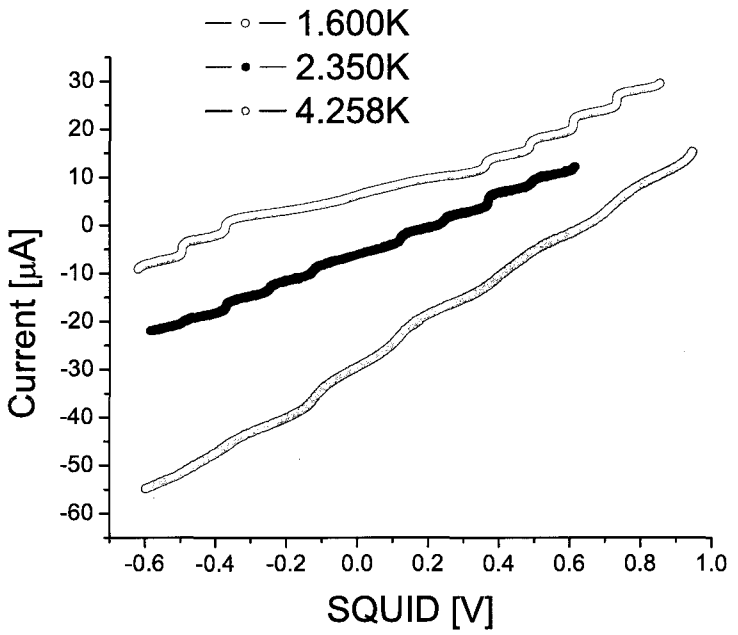

Figure 5.15: Shapiro steps of junction A at three temperature values. The curves have been offset along the current axis for clarity.

temperatures far from the 0-π temperature of a 0-π junction, we only measure integer steps. As we approach the transition temperature, we observe the onset of steps half-way between voltage intervals of the previous steps. As we can see from equation 5.18, it is the case that half-integer steps should exist at all temperatures for the intrinsic 4e-model, meaning there should be no such sudden frequency doubling of steps.

In both the 0-π junction model and the φ-junction model, half-integer Shapiro steps should only occur within a temperature range where it is valid to assume that the junction contains both π-state regions and 0-state regions. In the model of spatially non-uniform ferromagnetic barrier thickness, the valid temperature range is $T_\pi^{min} < T < T_\pi^{max}$, where T_π^{min} is the 0-π transition temperature of the thickest part of the junction, and T_π^{max} is the 0-π transition temperature of the thinest part of the junction. Based on the results of Frolov *et al.* [54], the appropriate temperature interval will be on the order of $\Delta T = 0.1K$.

Figure 5.15 shows I–V characteristics with microwave excitations at three

temperature values bracketing $T_\pi \approx 2.3K$ for sample A. The data has been offset along the current axis so that they don't overlap. Each trace was chosen from a series of power dependent curves to highlight the locations of the largest number of steps that were resolvable.

The data for junction C showed a number of features that made it difficult to extract exact values for the step height dependence as a function of applied power and temperature. At nearly every temperature, the steps were not vertical, but instead manifested as a slope change in the I–V characteristic. Also, we were unable to develop a technique for coupling the microwaves to the junction that would have allowed us to modulate the junction through several oscillation periods of the step heights.

The sample was designed with overlapping leads to reduce their inductance, and we speculate that this geometry led to a large capacitive coupling between the current injection leads that limited the size of the ac signal that could reach the junction.

However, the purpose of measuring the Shapiro steps for junction C was primarily to determine if there was a temperature dependence to the half-integer steps that is similar to the 0-π junction in figure 5.14.

To emphasize the location of the slope changes in the curves like 5.15 we used a numerical routine to evaluate the derivative of the data with respect to voltage. Then, slope changes in the I–V curves become sharp peaks in the effective (dI/dV) vs V curves.

Figure 5.16 shows the derivative of the three curves from figure 5.15. The temperature at which $I_c(T)$ was a minimum in junction C was approximately 2.30K. The blue and red data sets show peaks due to steps in the I–V data with the same frequency, while the yellow data shows peaks at half the frequency. Based on these results, we speculate that half-integer Shapiro steps appear over a temperature range of at least $\Delta T = 1.4K$ for sample C. That range is more than an order of magnitude larger than was measured for the 0-π junction.

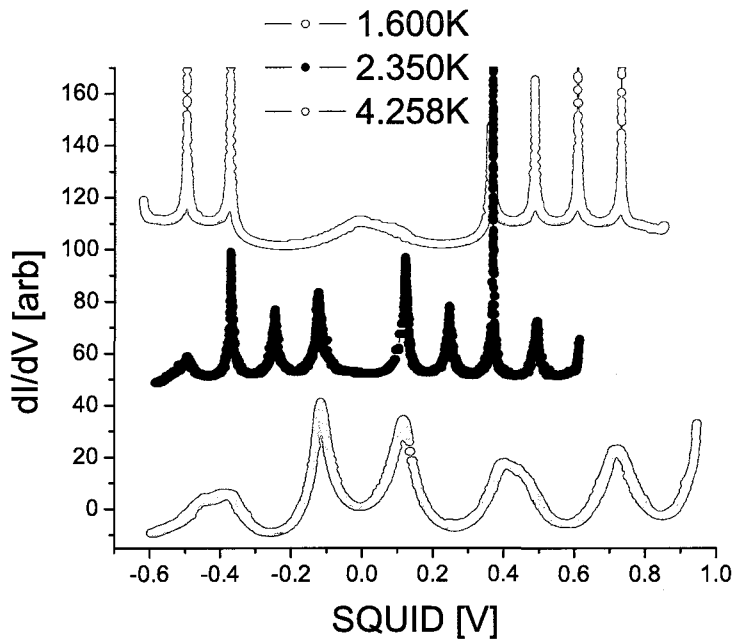

Figure 5.16: Computational derivative of Shapiro steps data for junction C. The blue curve is within 50mK of the temperature at which $I_c(T)$ is minimized. 0.7K away at $T = 1.60K$ (red curve), the Shapiro steps appear with the same frequency as near the crossover. By 1.9K away from the minimum temperature, the frequency of resolvable steps has fallen by a factor of 2 (gold curve).

Chapter 6

Phase-sensitive measurement of the current-phase relation

As was shown in chapter 5, there are several techniques for identifying second-order Josephson tunneling behavior using transport measurements. However, they fail to establish the relative signs of the first- and second-order tunneling coefficients, which we learned in chapter 4 is the easiest method for distinguishing between the four-electron tunneling model (4e model) and the inhomogeneous barrier model (φ-junction model). As a result, it is useful to identify a technique that can directly measure the current-phase relation of a junction.

6.1 SQUID interferometry technique

In chapter 2, we showed that the flux through a superconducting ring is quantized (this assumes a path in the superconducting electrode for which $J_s = 0$) due to the periodicity of the superconducting phase. The technique that we use to directly measure the current-phase relation is an extension of that flux quantization arguement.

In this measurement, we embed our Josephson junction in a superconducting ring, as shown schematically in figure 6.1. The single-junction in a ring geometry is commonly referred to as the rf SQUID. To calculate the expected response of this

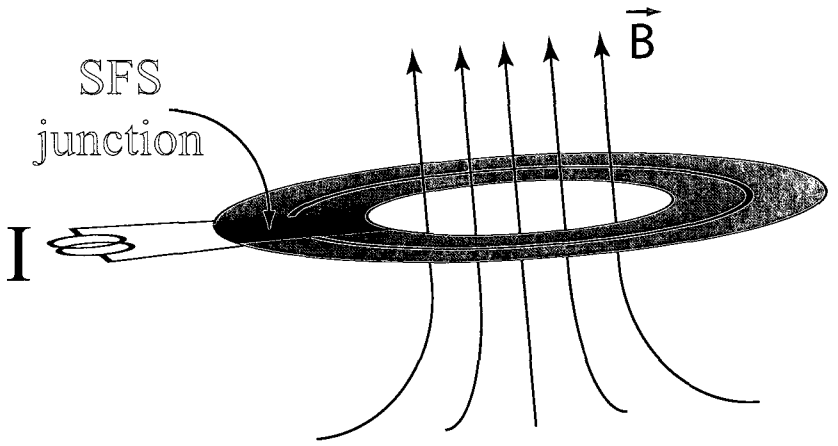

Figure 6.1: Shows an illustration of the rf SQUID geometry with leads for current injection. The blue ring is a superconducting film that is interrupted by the SFS Josephson junction, represented in red. Applied current creates a flux in the loop that is proportional to the phase drop across the junction.

system, we start by writing the phase drop across the junction in its invariant form,

$$\phi = \theta_1 - \theta_2 - \int_1^2 A \cdot dl, \tag{6.1}$$

where the line integral is taken along the shortest path across the junction.

To understand the relationship between the field through the loop and the phase difference across the junction, we again integrate the phase gradient around the loop (assuming I_s is zero). In the vicinity of the junction we use equation 6.1 for the phase drop with the result that $2\pi n = 2\pi(\Phi/\Phi_0) + \phi$. Solving for the phase difference across the junction and dropping extra terms of 2π gives

$$\phi = -2\pi\frac{\Phi}{\Phi_0}, \tag{6.2}$$

with corresponding supercurrent $-I_s(2\pi\Phi/\Phi_0)$. The negative sign indicates that the current flows in a direction to oppose the flux through the loop.

Experimentally it is easiest to apply current through leads across the junction and monitor the flux threading the loop. The current splits between the junction

and the inductance of the superconducting ring according to the equation:

$$\begin{aligned} I_{total} &= I_{junction} + I_{inductor} \\ &= I_s(\frac{2\pi\Phi}{\Phi_0}) + \frac{\Phi}{L}, \end{aligned} \tag{6.3}$$

where L is the total inductance of the superconducting loop.

An important parameter in this geometry is β_L – the inductance parameter – which is given by

$$\beta_L = \frac{2\pi I_c L}{\Phi_0}. \tag{6.4}$$

When the CPR has the usual sinusoidal dependence, the magnitude of the inductance parameter indicates the relative size of the sinusoidal oscillations to the linear increase in flux from the inductor. The red curves in figure 6.2 show flux as a function of applied current for several values of β_L in a junction that contains only $sin(\phi)$ terms.

In the case that $\beta_L > 1$, we see that the response is no longer single-valued in applied current. As a result, the flux data (simulated in black curves) show hysteretic jumps. The data as theorized would be obtained by performing a bipolar retrace of the current, i.e. ramp the current from $0 \rightarrow I_{max} \rightarrow I_{min} \rightarrow 0$. The bipolar method is what we use in real data-taking and why the curves show switches in both directions. We can see that it is necessary to make sure that $\beta_L < 1$ in order to map the full current-phase relation.

6.1.1 Experimental setup

The first implementations of this technique of embedding a junction in a superconducting loop were performed 40 years ago. Specifically, the dc technique of monitoring the magnetic flux in an rf SQUID as a function of applied current, was first implemented by Jackel *et al.* [72] and later refined by Waldram *et al.* [73]. Our approach is a modification of this technique.

In our application of the method, a commercial dc-SQUID (two Josephson

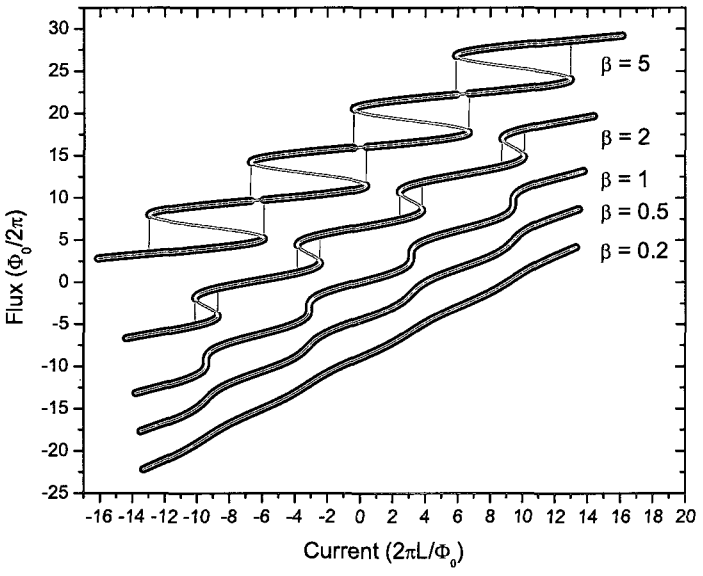

Figure 6.2: Simulated curves of the response of an rf SQUID circuit to applied current. The red lines represent the theoretical CPR for a junction containing only a first-order component, while the black data points represent the hysteretic data that one would expect to actually measure. The curves are offset along the y-axis for clarity.

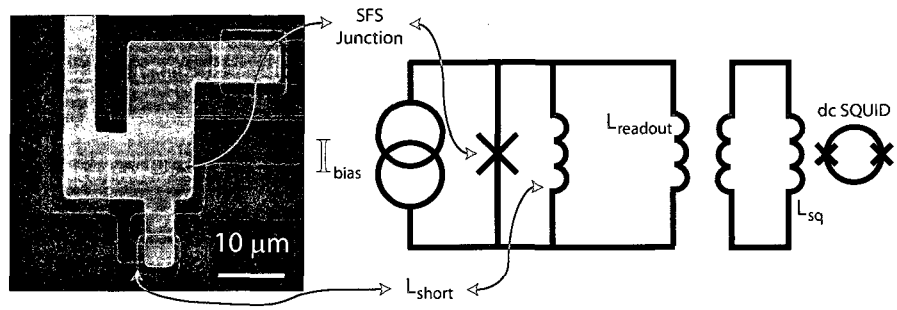

Figure 6.3: (Left) A photograph of a 2x2μm trilayer junction fabricated in the rf SQUID geometry for direct current–phase measurements. The current injection leads come in from the left, while the overlapping leads coming in from the top lead to the inductor used to measure flux. The small loop is a shorting inductor meant to reduce the inductance parameter β_L. (Right) The full circuit schematic for the rf SQUID circuit.

junctions in parallel in a superconducting loop) is used to monitor the magnetic flux. Figure 6.3 shows a schematic of our circuit.

Anticipating large critical currents, the sample geometry was chosen to minimize the effective inductance of the SQUID loop. Specifically, a small shorting inductor was placed in parallel with the large loop used to read out the flux in the SQUID circuit (L_{short} in figure 6.3). The smaller inductor was expected to be 2-4 orders of magnitude less than the readout inductor so that $L_{effective} = (1/L_{readout} + 1/L_{short})^{-1} \approx L_{short}$ and $\beta_L = 2\pi I_c L_{effective}/\Phi_0$.

The large inductor effectively draws a small fraction of the total circulating current away from the short for readout by the SQUID.

6.2 Results

In Chapter 5, we showed the results of transport measurements on the 2x2 μm junction with a persistent critical current of approximately 28 μA at the apparent T_π of 2.3K, which we called junction C. Chronologically, that junction was first measured in the rf SQUID configuration. Figure 6.4 shows the rf SQUID response of junction C at several different temperature values.

Several key differences exist between the simulation shown in figure 6.2 and the

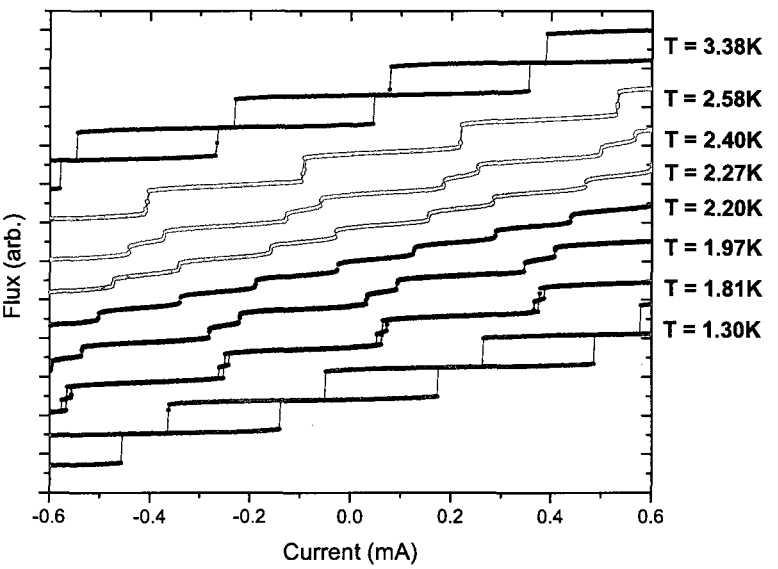

Figure 6.4: A temperature progression of the rf SQUID response of a 2x2μm^2 junction. The middle curve shows the 0- to π-state crossover temperature. As the temperature nears the 2.20K crossover, the frequency of oscillation doubles. The curves are offset along the y-axis for clarity only.

actual data. First, near the crossover temperature of 2.2K, the periodicity of the non-linear component of the response is half (the frequency of oscillations is double) that of the SQUID response at higher temperatures. This is the unambiguous signature of second-order harmonics appearing in the tunneling signature of this junction at the crossover temperature. As a result of the non-vanishing component in the tunneling current, the SQUID response remains hysteretic at all temperatures. Based on the linear part of these curves, we can measure the effective inductance of the superconducting loop as $H \approx 10pH$. From that, we can estimate the smallest inductance parameter, β_L for the circuit as:

$$\begin{aligned} \beta_L &= \frac{2\pi I_c L}{\Phi_0} \\ &\approx 1.06 \end{aligned} \tag{6.5}$$

For this value of β_L, we expect there should be hysteresis in the rf SQUID response data at all temperatures. Despite this, the curves from Figure 6.4 in the temperature interval of $1.97K \geq T \leq 2.58K$ seem to retrace perfectly. This effect is likely due to thermal excitations near the switching point that may cause the rf SQUID loop to jump between magnetic flux states early such that the failure to retrace seems to disappear before $\beta_L < 1$.

Another factor that further complicates understanding the signal hystersis is that some of the curves in this temperature range contain data points that lie between the apparent magnetic flux states. This is a data averaging effect that can be understood by closely examining the method used to acquire the curves. In order to reduce the effects of high-frequency noise in the readout SQUID, each magnetic flux data point in a curve is sampled approximately 100-500 times at each current step. For current values very near the thermally-induced switching point, the rf SQUID can oscillate between the higher flux state and lower flux state so that an average of many single-shot measurements will produce a value between the two allowed states.

Despite the hysteretic nature of the rf SQUID data shown in figure 6.4, we can fit these curves to extract the first-order and second-order Josephson critical currents. The technique we used to fit the curves was a least-squares regression method. The procedure is complicated by the apparent points near the switching events. We expect these points to be less strongly correlated to the real CPR than points far from switching events. The simplest way to account for this is to exclude points that appear in between switching events from the fits and to give equal weighting to all other points. For the fit, we used the equation:

$$I_{app} = A_0 V_{squid} + I_{c1} sin(A_1 V_{squid} + \delta) + I_{c2} sin[2(A_1 V_{squid} + \delta)] + I_0 \qquad (6.6)$$

where I_{app} is the applied current, V_{squid} is the measured voltage, and the rest of the variables represent the free parameters with the following meanings:

Parameter	Meaning
A_0	The slope of the linear part of the flux component. This represents (in units of SQUID readout voltage) the inductance of the rf SQUID loop.
A_1	The period of oscillation of the CPR in units of radians/volt.
I_{c1}	The magnitude of the $sin(\phi)$ component of the junction CPR.
I_{c2}	The magnitude of the $sin(2\phi)$ component of the junction CPR.
δ	An arbitrary phase factor meant to account for real offsets in the background field applied to the loop as well as virtual offsets due to the arbitrary zero-value of the SQUID readout sensor.
I_0	Offset in the zero-flux current value.

The curves from Figure 6.4 have been replotted in Figure 6.5 with the results of the fit for each overlayed in black on their respective data points. The linear portion of the fit, $A_0 V_{squid}$, has been removed from each of the data sets so that only the junction CPR remains.

The values of the free parameters for each of the curves is as follows:

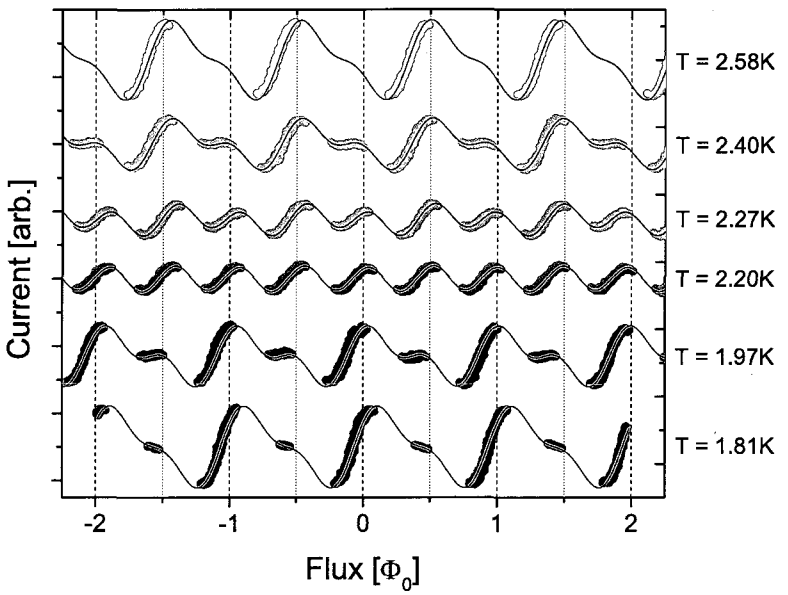

Figure 6.5: Extracted CPR curves as a function of temperature. The colored points show the data, while the black curves are fits to the data using both first– and second–order tunneling terms.

Temp (K)	A_0 (rad/volt)	I_{c1} (μA)	I_{c2} (μA)	A_1 (rad/volt)	δ (rad)	I_0 (A)
2.58	3.95e-4	98.5	38 (fixed)	1470.95	-0.212	1.04e-4
2.40	6.78e-4	54.1	34.1	1470.76	-0.278	6.85e-5
2.27	-3.64e-4	17.4	34.5	1473.03	-0.444	4.55e-5
2.20	-2.12e-4	-3.11	35.8	1482.73	-0.399	2.96e-5
1.97	-2.79e-6	-63.3e	40.6	1460.52	3.74	-8.74e-5
1.81	-7.93e-5	-116.2	38 (fixed)	1466.12	3.57	1.06e-4

Both A_0 and I_0 in the table above do not have the expected physical meaning of the loop inductance and dc current offset, respectively. The reason is that in order to increase the fitting speed and accuracy, a line, fit by eye, was subtracted from each of the curves before running the fitting algorithm. The result was the extracted CPR curve with a small, random slope and current offset which are the quantities listed as A_0 and I_0 in the table. As such, negative slope does not indicate a negative inductance but rather that the initial subtraction was of a line with a

slightly larger slope than the real value. The fit curves plotted in Figure 6.5 are the sinusoidal parts of the fit without the A_0, $A_1 V_{sq}$ or I_0 terms.

Based on several iterations of fitting the original rf-SQUID data, we can estimate the errors in the reported values of I_{c1} and I_{c2} – the quantities we are most interested in. For the first-order, I_{c1}, term, the error is approximately constant at all temperatures and equal to $\pm 5\mu$A. However, the size of the error is inversely related to the reported magnitude of the second-order term, I_{c2}. In other words, the error in the reported value of I_{c2} is highest at 1.97K. This relation is due to the fact that the hysteresis causes fewer data points for fitting. At 2.20K, the temperature at which the second-order term dominates the data, the error is approximately $\pm 5\mu$A – the same as for the first-order term.

6.2.1 Comparison to theory

At $T = 2.58K$ the hysteresis is too large to show any of the points associated with the $sin(2\phi)$ term, so the coefficient I_{c2} was set to $38\mu A$ (as an upper bound based on the middle temperature steps) before fitting the data. The same thing was done for the data, at $T = 1.81$, because the number of $sin(2\phi)$ points is very small.

The temperature dependence of I_{c1} and I_{c2} from the fits are plotted in figure 6.6, including the points that were fixed. The graph shows that over the temperature range where data for I_{c2} is available it is both positive and constant.

The fitting model given by equation 6.6 is based on the expected signature from either the 4e-model or the φ-junction model of second-order harmonics. It assumes that the $sin(\phi)$ term and the $sin(2\phi)$ terms cannot have an arbitrary phase shift relative to one another.

Adding an overall shift of π to δ makes the first-order term negative but has no effect on the second-order term, which corresponds to the junction being in the π-state. The fitting method does not require that the π-state corresponds to the low-temperature regime, but we expect this to be true based on previous imaging measurements on π-junction arrays that were also fabricated in Chernogolovka [74].

There is no overall phase shift that can be added to δ that changes the sign of

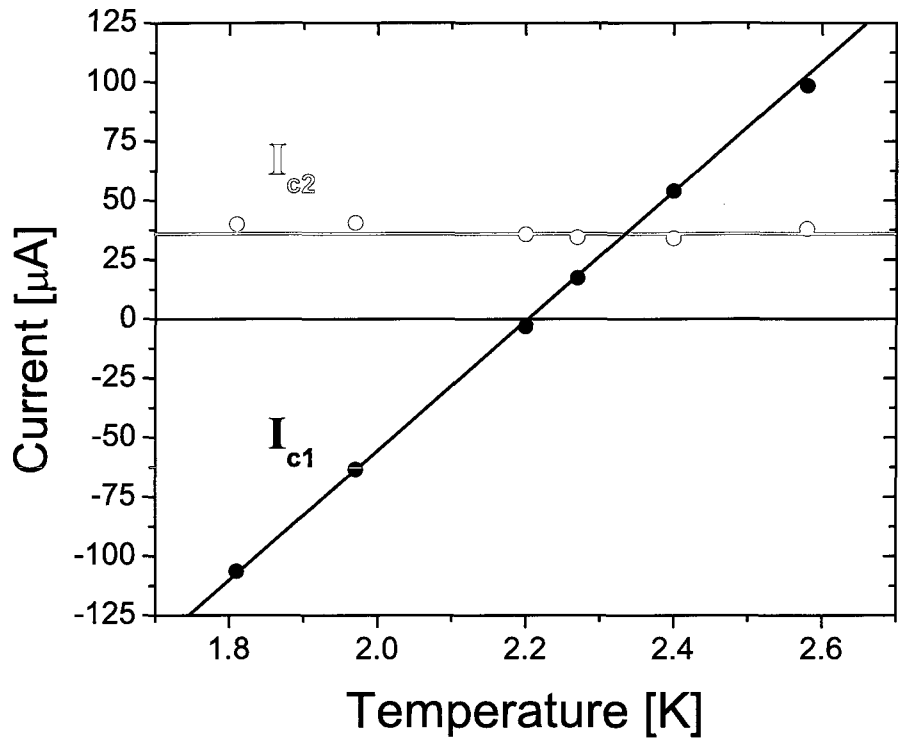

Figure 6.6: The coefficients of the first- (I_{c1}) and second-order (I_{c2}) harmonics from the fits to the rf SQUID data.

the I_{c2} term while leaving the I_{c1} term unaffected. As a result, this technique of measuring the current-phase relation gives the absolute sign for I_{c2} except in the limit that $I_{c1} = 0$. Then, adding a factor of $\pi/2$ to δ changes the sign of the coefficient without upsetting the fit.

Chapter 7

Conclusions

We have directly measured the current-phase relation of a superconductor-ferromagnet-superconductor (SFS) junction and showed that it contained a mixing of $sin(\phi)$ and $sin(2\phi)$ harmonics. Based on fits of our results, we have found that the coefficient of the first-order term, I_{c1}, transitions from positive to negative through zero as a function of temperature. Also, the second-order term, I_{c2}, remained positive and constant throughout the temperature regime where it was accessible.

In addition, we have shown that diffraction patterns on the same junction did not show the inhomogeneity previously seen in the 0-π junction, and that Shapiro steps measurements indicated the presence of half-integer steps of a temperature range of at least 2K.

Both the sign of the second-harmonic term and the wide temperature range over which half-integer Shapiro steps appeared indicated that the φ-junction model for a $sin(2\phi)$ component is not sufficient to account for the behavior of the junction.

7.1 Future work

The results we obtained suggest several avenues for further experimentation. The inductance parameter, β_L of the rf-SQUID experiment loop never became small enough for the entire current-phase relation to be accessible. It should be possible

to decrease the value of the shorting inductor in future samples by either decreasing its area or by shielding it with a superconducting ground plane. Eliminating the hysteresis in this way should cause the second-order term to be accessible over a wider temperature range.

Also, the magnitude of the persistent second-harmonic term was rather large, $\sim 0.1 I_{c1}^{max}$, which is inconsistent with what is expected from the coherent transfer of a four-electron state. Measuring the current-phase relation in a variety of samples in which barrier inhomogeneities were intentionally built in could be constructive.

If those experiments consistently resulted in a large, negative term proportional to $sin(2\phi)$, they could confirm the φ-junction model, and strengthen the case that our positive I_{c2} result shows a different effect.

References

[1] H. K. Onnes, Commun. Phys. Lab. Univ. Leiden **109**, 280 (1911).

[2] W. Meissner and R. Ochsenfeld, Naturwissenschaften **27**, 787 (1933).

[3] L. N. Cooper, Physical Review **104**, 1189 (1956).

[4] J. Bardeen, L. N. Cooper, and J. R. Schrieffer, Physical Review **108**, 1175 (1957).

[5] D. Pines, Physical Review **124c**, 280 (1958).

[6] E. Maxwell, Physical Review **78**, 477 (1950).

[7] C. A. Reynolds, B. Serin, W. H. Wright, and L. B. Nesbitt, Physical Review **78**, 487 (1950).

[8] V. L. Ginzburg and L. D. Landau, Zh. Eksp. Teor. Fiz. **20**, 1064 (1950).

[9] F. London and H. London, Proc. Roy. Soc. **A141**, 547 (1935).

[10] J. R. Waldram, *Superconductivity of Metals and Cuprates*, 1st ed. (Institute of Physics Publishing, 1996).

[11] B. D. Josephson, Physical Letters **1**, 251 (1962).

[12] A. A. Golubov, M. Y. Kupriyanov, and E. Il'ichev, Reviews of Modern Physics **76**, 411 (2004).

[13] K. K. Likharev, Reviews of Modern Physics **51**, 101 (1979).

[14] V. Ambegaokar and A. Baratoff, Physical Review Letters **10**, 486 (1963).

[15] L. N. Bulaevskii, V. V. Kuzii, and A. A. Sobyanin, Journal of Experimental and Theoretical Physics Letters **25**, 290 (1977).

[16] A. A. Abrikosov and L. P. Gor'kov, Journal of Experimental and Theoretical Physics **10**, 593 (1960).

[17] L. I. Glazman and K. A. Matveev, Journal of Experimental and Theoretical Physics Letters **49**, 659 (1989).

[18] F. Siano and R. Egger, Physical Review Letters **93**, 047002 (2004).

[19] A. F. Volkov, Physical Review Letters **74**, 4730 (1995).

[20] Y. S. Barash, H. Burkhardt, and D. Rainer, Physical Review Letters **77**, 4070 (1996).

[21] T. Lofwander, V. S. Shumeiko, and G. Wendin, Superconductor Science and Technology **14**, R53 (2001).

[22] A. I. Buzdin, L. N. Bulaevskii, and S. V. Panjukov, Journal of Experimental and Theoretical Physics **35**, 178 (1982).

[23] J. Bardeen and J. L. Johnson, Physical Review B **5**, 72 (1972).

[24] A. A. Zubkov and M. Y. Kupriyanov, Soviet Journal of Low Temperature Physics **9**, 279 (1983).

[25] T. T. Heikkila, F. K. Wilhelm, and G. Schon, Europhysical Letters **51**, 434 (2000).

[26] Z. Radovic, L. Dobrosavljevic-Grujic, and B. Vujicic, Physical Review B **63**, 214512 (2001).

[27] A. Buzdin, Physical Review B **72**, 100501(R) (2005).

[28] M. Houzet, V. Vinokur, and F. Pistolesi, Physical Review B **72**, 220506(R) (2005).

[29] V. V. Ryazanov *et al.*, Physical Review Letters **65**, 22413 (2001).

[30] E. A. Demler, G. B. Arnold, and M. R. Beasley, Physical Review B **55**, 15174 (1997).

[31] A. I. Buzdin, Reviews of Modern Physics **77**, 935 (2005).

[32] C. Kittel, *Introduction to Solid State Physics*, 7th ed. (John Wiley and Sons, Inc, 1996).

[33] V. L. Ginzburg and L. D. Landau, Soviet Physics Journal of Experimental and Theoretical Physics **4**, 153 (1956).

[34] D. Saint-James, G. Sarma, and E. J. Thomas, *Type II Superconductivity* (Pergamon Press, 1969).

[35] P. Fulde and R. Ferrell, Physical Review **135**, A550 (1964).

[36] A. I. Larkin and Y. N. Ovchinnikov, Soviet Physics Journal of Experimental and Theoretical Physics **20**, 762 (1965).

[37] V. V. Ryazanov *et al.*, Usp. Fiz. Nauk (Suppl.) **171**, 81 (2001).

[38] A. Buzdin, Physical Review B **62**, 11377 (2000).

[39] T. Kontos, M. Aprili, J. Lesueur, and X. Grison, Physical Review Letters **86**, 304 (2000).

[40] T. Kontos, M. Aprili, J. Lesueur, X. Grison, and L. Dumoulin, Physical Review Letters **93**, 137001 (2004).

[41] A. I. Buzdin and M. Y. Kupriyanov, Journal of Experimental and Theoretical Physics **52**, 487 (1990).

[42] V. V. Ryazanov, V. A. Oboznov, A. S. Prokofiev, V. V. Bolginov, and A. K. Feofanov, Journal of Low Temperature Physics **136**, 385 (2004).

[43] J. S. Jiang, D. Davidovic, D. H. Reich, and C. L. Chien, Physical Review Letters **74**, 314 (1995).

[44] V. A. Oboznov, V. V. Bolginov, A. K. Feofanov, V. V. Ryazanov, and A. I. Buzdin, Physical Review Letters **96**, 197003 (2006).

[45] T. Kontos *et al.*, Physical Review Letters **89**, 173007 (2002).

[46] H. Sellier, C. Baraduc, F. Lefloch, and R. Calemczuk, Physical Review B **68**, 054531 (2003).

[47] G. Eilenberger, Zeitschrift Fur Physik **214**, 196 (1968).

[48] A. I. Buzdin and M. Y. Kupriyanov, Journal of Experimental and Theoretical Physics **53**, 321 (1991).

[49] K. D. Usadel, Physical Review Letters **25**, 507 (1970).

[50] Y. Blum, A. Tsukernik, M. Karpovski, and A. Palevski, Physical Review Letters **89**, 187004 (2002).

[51] C. Bell, R. Loloee, G. Burnell, and M. G. Blamire, Physical Review B **71**, 180501(R) (2005).

[52] J. W. A. Robinson, S. Piano, G. Burnell, C. Bell, and M. Blamire, Physical Review Letters **97**, 177003 (2006).

[53] S. M. Frolov, *Current-Phase Relations of Josephson Junctions with Ferromagnetic Barriers*, PhD thesis, University of Illinois at Urbana-Champaign, 2005.

[54] S. M. Frolov, D. J. Van Harlingen, V. V. Bolginov, V. A. Oboznov, and V. V. Ryazanov, Physical Review B **74**, 020503(R) (2006).

[55] S. M. Frolov, D. J. Van Harlingen, V. A. Oboznov, V. V. Bolginov, and V. V. Ryazanov, Physical Review B **70**, 144505 (2004).

[56] J. J. A. Baselmans, A. F. Morpurgo, B. J. van Wees, and T. M. Klapwijk, Nature **397**, 43 (1999).

[57] N. M. Chtchelkatchev, W. Belzig, Y. Y. Nazarov, and C. Bruder, Journal of Experimental and Theoretical Physics Letters **74**, 323 (2001).

[58] F. Romeo and R. D. Luca, Physical Letters A **328**, 330 (2004).

[59] K. Lehnert *et al.*, Physical Review Letters **82**, 330 (1999).

[60] M. Fuechsle *et al.*, Physical Review Letters **102**, 127001 (2009).

[61] M. Weides *et al.*, Physical Review Letters **97**, 247001 (2006).

[62] R. G. Mints, Physical Review B **57**, 3221(R) (1998).

[63] R. G. Mints and I. Papiashvili, Physical Review B **62**, 15214 (2000).

[64] R. G. Mints and I. Papiashvili, Physical Review B **64**, 134501 (2001).

[65] R. G. Mints and I. Papiashvili, Superconductor Science and Technology **15**, 307 (2002).

[66] A. Buzdin and A. E. Koshelev, Physical Review B **67**, 220504(R) (2003).

[67] A. Barone and G. Paterno, *Physics and Applications of the Josephson Effect*, 1st ed. (John Wiley and Sons, Inc, 1982).

[68] D. J. Van Harlingen, Reviews of Modern Physics **67**, 515 (1995).

[69] E. Goldobin, D. Koelle, R. Kleiner, and A. Buzdin, Physical Review B **76**, 224523 (2007).

[70] S. Shapiro, Physical Review Letters **80**, 80 (1963).

[71] M. Moshe and R. G. Mints, Physical Review B **76**, 054518 (2007).

[72] L. D. Jackel, R. A. Buhrman, and W. W. Webb, Physical Review B **10**, 2782 (1974).

[73] J. R. Waldram and J. M. Lumley, Revue de Physique Appliquee **10**, 7 (1975).

[74] S. M. Frolov *et al.*, Nature Physics **4**, 32 (2007).

Author's Biography

Micah John Atman Stoutimore was born in Vernal, Utah, on February 5, 1979, during a transitory time in his parents life. By July of 1980, Micah's brother, Zachariah, was born in Colorado and in the fall of 1981 the whole family was in Gainesville, Florida, where both parents ultimately completed graduate school at the University of Florida.

From a young age, Micah took schoolwork very seriously. So much so, that his parents decided to enroll him in an alternative kindergarten in the hopes of easing his concern over the pending course load. Throughout school and life, Micah showed an interest and aptitude particularly in mathematics and the physical sciences.

During his senior year of high school, Micah had one of those teachers who changes lives, and he taught physics. As a result, Micah made it a point to enroll in physics despite pursuing a bachelor's degree in electrical engineering at the University of Florida. As it often does, one thing led to another, and Micah found himself graduating with a degree in physics and a desire to face the challenge of graduate school at the University of Illinois at Urbana-Champaign.

Once there, Micah was attracted to the strange and interesting physics of superconductivity by his mentor, Dale Van Harlingen. After attempting a few projects with varying levels of success, Micah was guided to the wonderful physics of superconductor-ferromagnet-superconductor Josephson junctions, which led to his Ph.D. thesis.

As a postdoctoral researcher at the University of Maryland at College Park, Micah will continue studying the physics of Josephson junctions in the context of quantum computing. Micah is certain that he will continue to grow and learn as a

scientist in the capable and energetic company of Chris Lobb and Kevin Osborn among many others at UMD, JQI, NIST and several other prestigious acronyms. Micah also hopes to learn something of the "nature of knowledge," which is how one close friend and trusted colleague has described quantum information science.